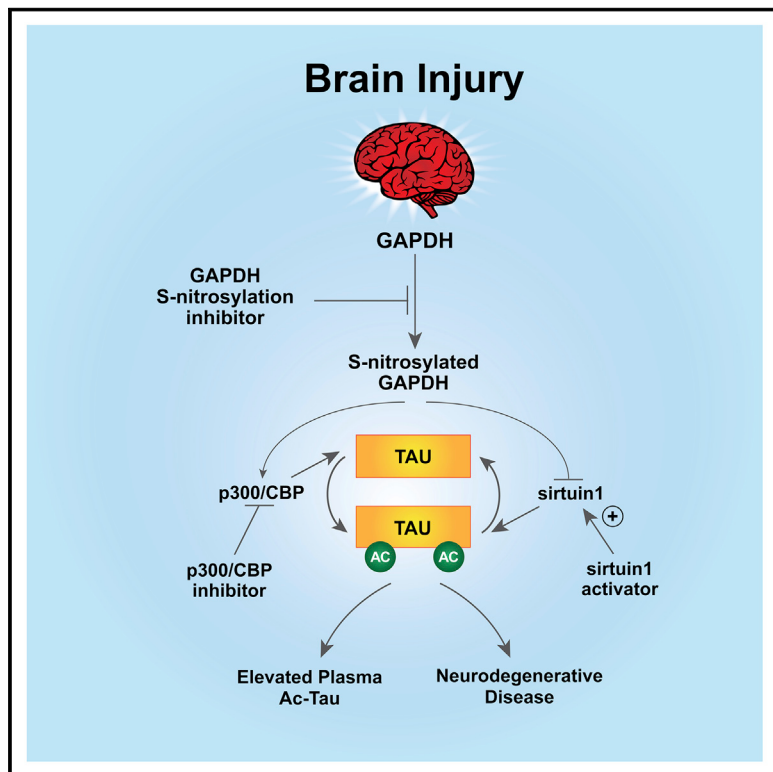


# Reducing acetylated tau is neuroprotective in brain injury

## Graphical abstract



## Authors

Min-Kyoo Shin, Edwin Vázquez-Rosa,  
Yeojeung Koh, ..., Feixiong Cheng,  
James D. Reynolds, Andrew A. Pieper

## Correspondence

andrew.pieper@harringtondiscovery.org

## In brief

Reducing brain injury-induced neuronal tau acetylation is neuroprotective in traumatic brain injury and has a role in Alzheimer's disease pathogenesis.

## Highlights

- Brain injury induces Alzheimer's disease-like neuronal ac-tau
- Neurodegenerative brain injury is reflected by ac-tau blood levels in mice and people
- Decreasing ac-tau after brain injury at multiple signaling nodes is neuroprotective
- Ac-tau-inhibiting medicines are associated with reduced neurodegenerative disease



## Article

# Reducing acetylated tau is neuroprotective in brain injury

Min-Kyoo Shin,<sup>1,2,3,4,31</sup> Edwin Vázquez-Rosa,<sup>1,2,3,4,31</sup> Yeojung Koh,<sup>1,2,3,4</sup> Matasha Dhar,<sup>1,2,3,4</sup> Kalyani Chaubey,<sup>1,2,3,4</sup> Coral J. Cintrón-Pérez,<sup>1,2,3,4</sup> Sarah Barker,<sup>1,2,3,4</sup> Emiko Miller,<sup>1,2,3,4</sup> Kathryn Franke,<sup>1,2,3,4</sup> Maria F. Noterman,<sup>5</sup> Divya Seth,<sup>4,6</sup> Rachael S. Allen,<sup>7,8</sup> Cara T. Motz,<sup>7,8</sup> Sriganesh Ramachandra Rao,<sup>9,10</sup> Lara A. Skelton,<sup>9,10</sup> Machelle T. Pardue,<sup>7,8</sup> Steven J. Fliesler,<sup>9,10</sup> Chao Wang,<sup>11</sup> Tara E. Tracy,<sup>12</sup> Li Gan,<sup>13</sup> Daniel J. Liebl,<sup>14</sup> Jude P.J. Savarraj,<sup>15</sup>

(Author list continued on next page)

<sup>1</sup>Harrington Discovery Institute, University Hospitals Cleveland Medical Center, Cleveland, OH, USA

<sup>2</sup>Department of Psychiatry, Case Western Reserve University, Cleveland, OH, USA

<sup>3</sup>Geriatric Psychiatry, GRECC, Louis Stokes Cleveland VA Medical Center; Cleveland, OH, USA

<sup>4</sup>Institute for Transformative Molecular Medicine, School of Medicine, Case Western Reserve University, Cleveland, OH, USA

<sup>5</sup>Department of Psychiatry, University of Iowa Carver College of Medicine, Iowa City, IA, USA

<sup>6</sup>Department of Medicine, University Hospitals Cleveland Medical Center, Cleveland, OH, USA

<sup>7</sup>Center for Visual and Neurocognitive Rehabilitation, Atlanta VA Healthcare System, Atlanta, GA, USA

<sup>8</sup>Department of Biomedical Engineering, Georgia Institute of Technology, Atlanta, GA, US

<sup>9</sup>Departments of Ophthalmology and Biochemistry, and the Neuroscience Graduate Program, SUNY-University at Buffalo, Buffalo, NY, USA

<sup>10</sup>Research Service, VA Western NY Healthcare System, Buffalo, NY, USA

<sup>11</sup>Gladstone Institute of Neurological Disease, San Francisco, CA, USA

<sup>12</sup>The Buck Institute, Novato, CA, USA

<sup>13</sup>Helen and Robert Appel Alzheimer's Disease Research Institute, Weill Cornell Medicine, New York, NY, USA

<sup>14</sup>The Miami Project to Cure Paralysis, Department of Neurological Surgery, University of Miami Miller School of Medicine, Miami, FL, USA

<sup>15</sup>Department of Neurosurgery, McGovern Medical School, The University of Texas Health Science Center at Houston, Houston, TX, USA

<sup>16</sup>Department of Neurology, McGovern Medical School, The University of Texas Health Science Center at Houston, Houston, TX, USA

<sup>17</sup>Department of Biomedical Informatics, College of Medicine, Ohio State University, Columbus, OH, USA

<sup>18</sup>Genomic Medicine Institute, Lerner Research Institute, Cleveland Clinic, Cleveland, OH, USA

<sup>19</sup>Department of Biochemistry, UT Southwestern Medical Center, Dallas, TX, USA

<sup>20</sup>MetroHealth Rehabilitation Institute, The MetroHealth System, Cleveland, OH

(Affiliations continued on next page)

## SUMMARY

Traumatic brain injury (TBI) is the largest non-genetic, non-aging related risk factor for Alzheimer's disease (AD). We report here that TBI induces tau acetylation (ac-tau) at sites acetylated also in human AD brain. This is mediated by S-nitrosylated-GAPDH, which simultaneously inactivates Sirtuin1 deacetylase and activates p300/CBP acetyltransferase, increasing neuronal ac-tau. Subsequent tau mislocalization causes neurodegeneration and neurobehavioral impairment, and ac-tau accumulates in the blood. Blocking GAPDH S-nitrosylation, inhibiting p300/CBP, or stimulating Sirtuin1 all protect mice from neurodegeneration, neurobehavioral impairment, and blood and brain accumulation of ac-tau after TBI. Ac-tau is thus a therapeutic target and potential blood biomarker of TBI that may represent pathologic convergence between TBI and AD. Increased ac-tau in human AD brain is further augmented in AD patients with history of TBI, and patients receiving the p300/CBP inhibitors salsalate or diflunisal exhibit decreased incidence of AD and clinically diagnosed TBI.

## INTRODUCTION

Traumatic brain injury (TBI) is typically caused by motor vehicle crashes, falls, contact sports, or assaults. The annual incidence of TBI in the United States alone is ~3.5 million, with ~5 million people currently living with TBI-related disabilities at an annual cost of ~\$80 billion (Centers for Disease Control and Prevention,

2015; Ma et al., 2014). At present, treatments for TBI focus on patient stabilization and mitigation of symptoms, and there are no medicines that specifically target the pathophysiological processes that drive neurodegeneration after brain injury. TBI also significantly increases the risk of later developing Alzheimer's disease (AD) (Johnson et al., 2010; Li et al., 2017). This suggests common pathologic mechanisms, and emerging evidence



Glenda L. Torres,<sup>15</sup> Hilda Ahnstedt,<sup>16</sup> Louise D. McCullough,<sup>16</sup> Ryan S. Kitagawa,<sup>15</sup> H. Alex Choi,<sup>15</sup> Pengyue Zhang,<sup>17</sup> Yuan Hou,<sup>18</sup> Chien-Wei Chiang,<sup>17</sup> Lang Li,<sup>17</sup> Francisco Ortiz,<sup>19</sup> Jessica A. Kilgore,<sup>19</sup> Noelle S. Williams,<sup>19</sup> Victoria C. Whitehair,<sup>20,21</sup> Tamar Gefen,<sup>22,23</sup> Margaret E. Flanagan,<sup>23,24</sup> Jonathan S. Stamler,<sup>1,4,6</sup> Mukesh K. Jain,<sup>1,6</sup> Allison Kraus,<sup>25</sup> Feixiong Cheng,<sup>18,26,27</sup> James D. Reynolds,<sup>1,4,28</sup> and Andrew A. Pieper<sup>1,2,3,4,29,30,32,\*</sup>

<sup>21</sup>Department of Physical Medicine and Rehabilitation, Case Western Reserve University, School of Medicine, Cleveland, OH USA

<sup>22</sup>Department of Psychiatry and Behavioral Sciences, Feinberg School of Medicine, Northwestern University, Chicago, IL, USA

<sup>23</sup>Mesulam Center for Cognitive Neurology and Alzheimer's Disease, Feinberg School of Medicine, Northwestern University, Chicago, IL, USA

<sup>24</sup>Department of Pathology, Northwestern University, Chicago, IL, USA

<sup>25</sup>Department of Pathology, Case Western Reserve University, School of Medicine, Cleveland, OH, USA

<sup>26</sup>Case Comprehensive Cancer Center, Case Western Reserve University School of Medicine, Cleveland, OH, USA

<sup>27</sup>Department of Molecular Medicine, Cleveland Clinic Lerner College of Medicine, Case Western Reserve University, Cleveland, OH, USA

<sup>28</sup>Departments of Anesthesiology & Perioperative Medicine, University Hospitals Cleveland Medical Center, Cleveland, OH, USA

<sup>29</sup>Weill Cornell Autism Research Program, Weill Cornell Medicine of Cornell University, New York, NY, USA

<sup>30</sup>Department of Neuroscience, Case Western Reserve University, School of Medicine, Cleveland, OH, USA

<sup>31</sup>These authors contributed equally

<sup>32</sup>Lead contact

\*Correspondence: andrew.pieper@harringtondiscovery.org

<https://doi.org/10.1016/j.cell.2021.03.032>

points to S-nitrosylation and acetylation (Uehara et al., 2006; Nakamura and Lipton, 2020; Sen et al., 2018). Indeed, a small post-mortem study recently reported increased acetylation of tau at lysine (K) 280 in the brains of three patients with AD and three patients with chronic traumatic encephalopathy (Lucke-Wold et al., 2017). In a separate study, the same rise in ac-tau at K280 was documented in the brains of ten additional patients with AD, five patients with corticobasal degeneration, and five patients with progressive supranuclear palsy (Irwin et al., 2012). Tau acetylation at both K274 and K281 was additionally reported in upwards of a dozen patients with severe AD (Tracy et al., 2016). However, these studies did not establish the driving forces or pathologic significance of the findings. Given the inter-relationship between TBI and AD, we sought to determine whether elevated ac-tau was a causal pathophysiologic factor in TBI, and thus a potential locus of convergence, and if so, then whether this might provide an experimental platform to understand *in vivo* pathophysiology related to ac-tau in the brain.

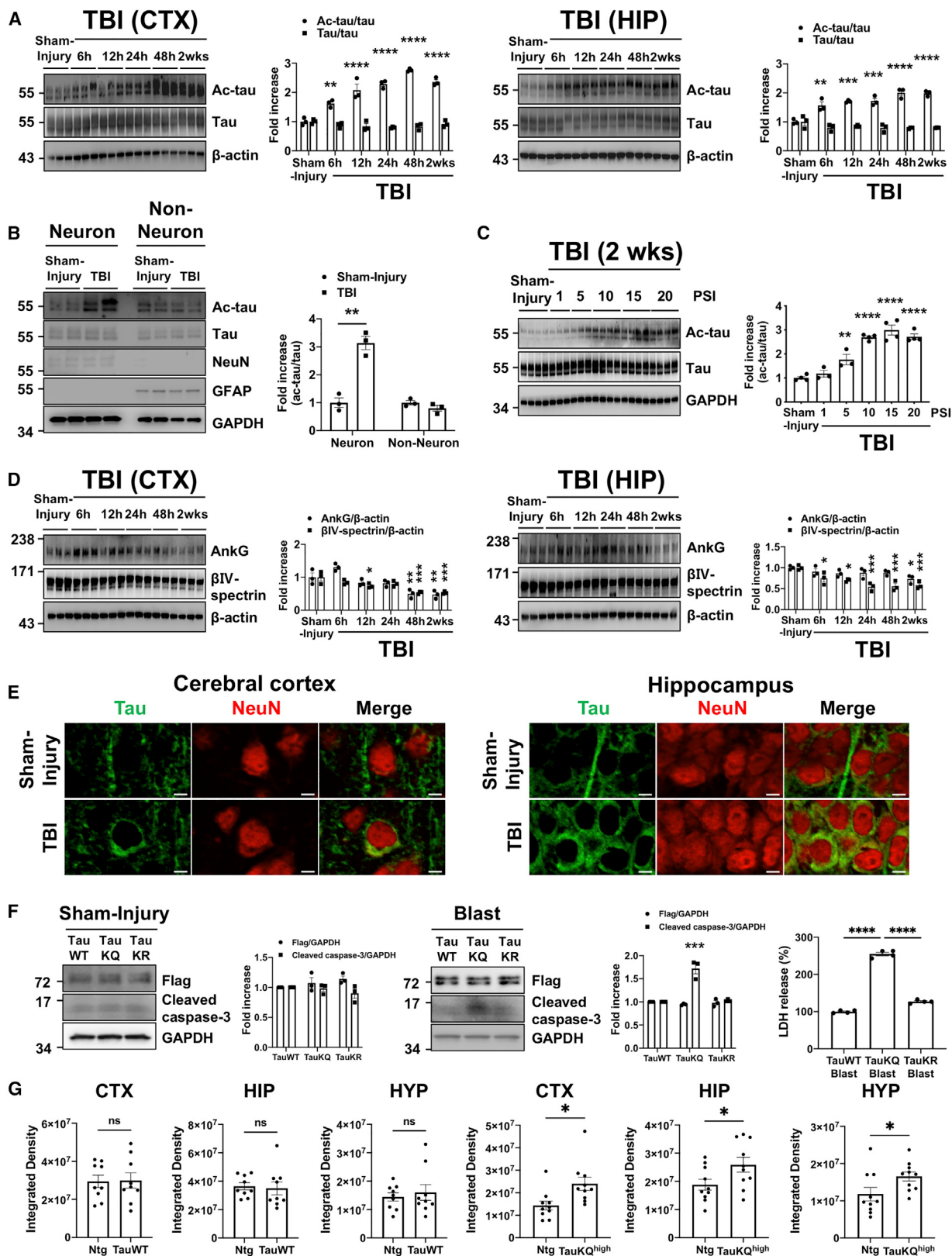
## RESULTS

### Brain injury induces neuronal tau acetylation

To begin, we employed a mouse model of multimodal TBI incorporating global concussive impact, acceleration/deceleration, and early-phase blast wave exposure (Shin et al., 2021). This model produces a complex brain injury with neurodegeneration and neurobehavioral impairment, beginning with acute axonal degeneration that persists chronically and eventually leads to blood-brain barrier degradation and nerve cell death (Yin et al., 2014, 2016; Dutca et al., 2014; Vázquez-Rosa et al., 2019, 2020; Wattiez et al., 2021). Already an established preclinical model of TBI, its clinical relevance is further strengthened here through nonbiased whole metabolomic analysis. Specifically, 1 week after injury, mice displayed altered plasma levels of fatty acids, amino acids, 5-oxoproline, and tricarboxylic acid cycle metabolites (Figure S1A), resembling published data from nonbiased plasma metabolomic analysis of human TBI (Orešić et al., 2016).

Using antibodies to mouse acetylated-tau (ac-tau) at K263 and K270 (Min et al., 2010; Figure S1B), which correspond respectively to human tau K274 and K281, we observed rapid and specific elevation of ac-tau in both the cerebral cortex and hippocampus of the brain after injury (Figure 1A). Importantly, the increased ac-tau was observed selectively in neurons of the brain (Figure 1B) and correlated with injury intensity (Figure 1C), while total tau levels remained unchanged (Figures 1A–1C). Our observation of the low-level presence of tau in non-neuronal cell types is consistent with previous reports (<http://www.brainrnaseq.org>; Perea et al., 2019; Bolós et al., 2017), and no change in non-neuronal tau was noted as a function of injury. The injury-dependent increase in neuronal ac-tau was observed in both males and females (Figure S1C) and also generalized to multiple forms and stages of TBI. For example, we determined that this is not only an acute, but also a chronic response to injury, as ac-tau remained elevated 17 months after injury in mice (Figure S1D). Ac-tau was also elevated 7 months after acoustic blast overpressure TBI in rats (Figure S1E), and at a range of times after controlled cortical impact TBI in mice (Figure S1F). In addition, ac-tau was acutely elevated in cerebellum after multimodal TBI (Figure S1G), but not in hypothalamus (Figure S1H), consistent with the previous observation of hypothalamic resistance to neurodegeneration in this model (Yin et al., 2014).

By contrast, tau phosphorylation after brain injury was unchanged at S202 (Figures S2A and S2B), which is part of the basis for AD Braak staging (Neddens et al., 2018), and reduced at S396 and S404, sites that mediate tau's ability to polymerize tubulin (Evans et al., 2000; Figures S2A and S2B). Tau phosphorylation was also somewhat reduced at S262 (Figures S2A and S2B). Although phosphorylation of S262 has been linked to tau acetylation in other contexts (Cook et al., 2014), inhibiting tau acetylation after brain injury had no effect on S262 phosphorylation (Figure S2C). Taken together, the data suggest a prominent role for tau acetylation and a lesser role for tau phosphorylation in the acute period following brain injury. Notably, the post-injury increase in ac-tau was also not associated with tau seeding (Figures S2D and S2E), nor with reduced expression of postsynaptic



kidney/brain (KIBBRA) protein (Figures S2F–S2I), a previously suggested consequence of tau acetylation (Tracy et al., 2016).

### Injury-induced neuronal tau acetylation leads to axon initial segment degradation and pathologic tau mislocalization

Clues to the possible function of ac-tau in brain injury were uncovered from published post-mortem studies of AD patients' brains, in which the magnitude of K274 and K281 acetylation correlated inversely with amounts of ankyrin-G (AnkG) and  $\beta$ IV-spectrin (Sohn et al., 2016), principle components of the axon initial segment (AIS). The AIS normally maintains neuronal health and limits tau distribution predominantly to axons (Schafer et al., 2009). After injury, we observed a rapid reduction in the levels of AnkG and  $\beta$ IV-spectrin (Figure 1D) that correlated with amounts and time course of increased tau acetylation (Figure 1A). AIS degradation also led to pathologic tau mislocalization into the somatodendritic compartment of neurons throughout the brain (Figure 1E).

To determine whether ac-tau was directly toxic to neurons, both *in vitro* and *in vivo* genetic tests were conducted. To begin, transfection of cultured human neuroblasts with either human tau acetylation mimetic or acetylation-resistant human tau showed that tau acetylation specifically increased neuronal cell death in an *in vitro* model of TBI, as measured by both cleaved caspase 3 and lactate dehydrogenase (LDH) release assay (Figure 1F). For *in vivo* investigation, a mouse correlate of this model, known as tauKQ<sup>high</sup> mice, was used. These transgenic mice express human tau with lysine-to-glutamine mutations that mimic acetylation at K274 and K281, which correspond to mouse K263 and K270, respectively. TauKQ<sup>high</sup> mice have been previously shown to exhibit memory deficits and impaired long-term potentiation (Tracy et al., 2016). Here, ~1-year-old tauKQ<sup>high</sup> mice displayed a significant degree of axonal degeneration, which was not observed in either nontransgenic wild-type littermates or human wild-type tau transgenic mice (Figures 1G, S2J, and S2K). The interesting observation that the hypothalamus of tauKQ<sup>high</sup> mice showed prominently increased axonal neurodegeneration contrasts with previously noted protection of this region in TBI (Yin et al., 2014). This suggests that the hypothalamus in mice may be physically protected from injury relative to other

regions of the brain, rather than composed of a subpopulation of neurons endowed with unique protective properties. Synaptic integrity in these animals was also assessed, through immunohistochemical staining for synaptic vesicle protein 2 (SV2). As shown in Figure S2L, tauKQ<sup>high</sup> mice displayed reduced SV2 in the hippocampus relative to nontransgenic wild-type littermates. Taken together, these results indicate that human ac-tau is directly toxic to neurons, both *in vitro* and *in vivo* in the brain.

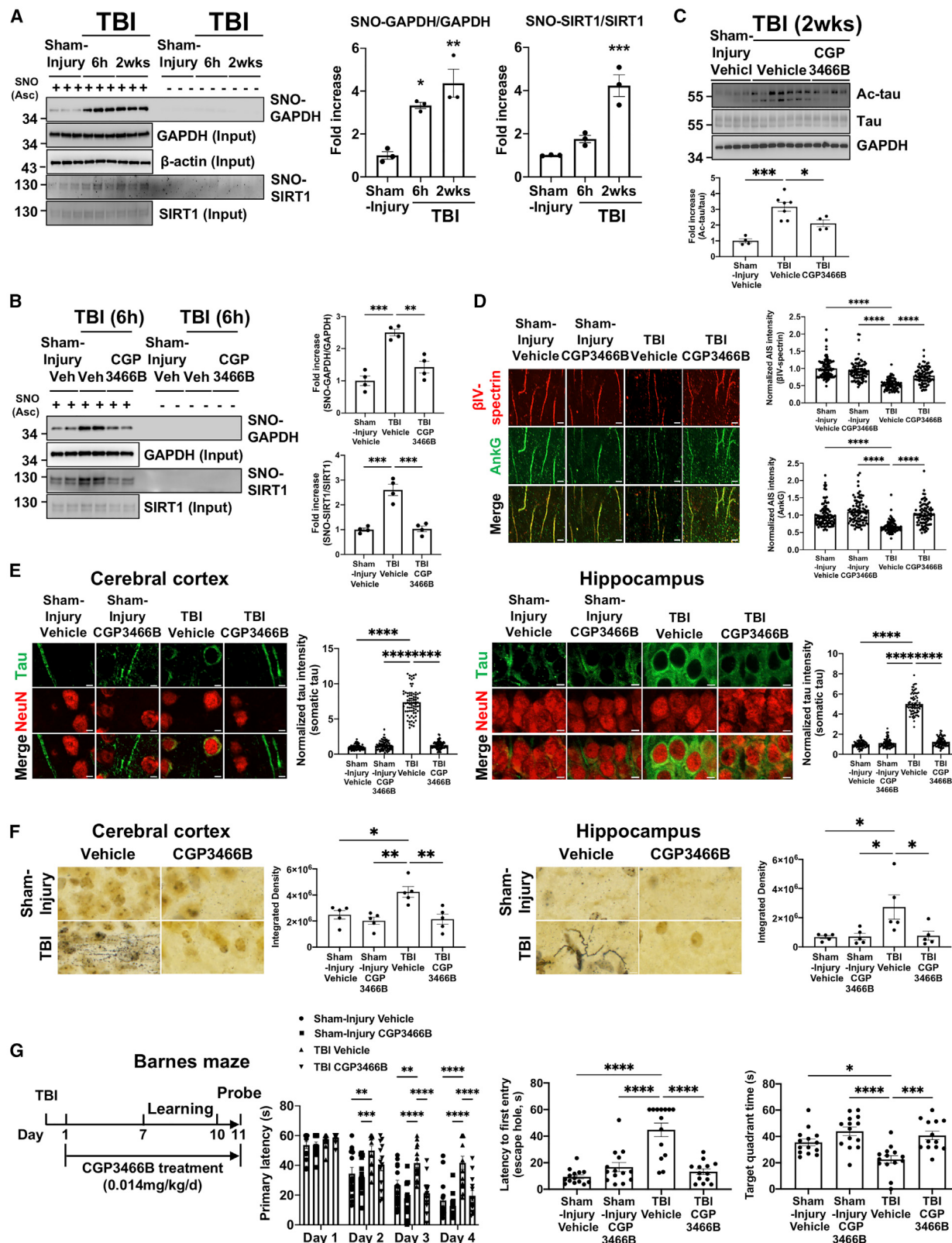
### Injury-induced neuronal tau acetylation is driven by non-canonical signaling

In cellular models of AD, protein acetylation has been linked to S-nitrosylation of GAPDH, which coordinately enhances p300/CBP acetyltransferase activity and inhibits Sirtuin1 (Sirt1) deacetylase activity to increase overall amounts of acetylation. Inhibitory S-nitrosylation of Sirt1 is mediated by aberrant transnitrosylase activity of GAPDH, whereas S-nitrosylated-GAPDH (SNO-GAPDH) also stimulates activation and acetylation of p300/CBP acetyltransferase (Hara and Snyder, 2006; Kornberg et al., 2010; Sen et al., 2018). After TBI, we found that both GAPDH and Sirt1 were S-nitrosylated (Figure 2A). Increased protein acetylation was further confirmed by measuring acetylation of histone H2AK5, a p300/CBP and Sirt1 substrate (Figures S3A and S3B). Initiation of daily treatment 15 min after injury with CGP3466B (0.014 mg/kg intraperitoneal [IP]), a specific inhibitor of GAPDH nitrosylation also known as omigapil (Waldmeier et al., 2000), blocked S-nitrosylation of both GAPDH and Sirt1 (Figures 2B and S3C). Furthermore, protein or activity levels of histone deacetylase 6 (HDAC6), which can deacetylate tau (Cohen et al., 2011; Cook et al., 2014), did not change at any of the time points after TBI (Figure S3D). Blocking GAPDH S-nitrosylation also reduced ac-tau and ac-p300/CBP (Figures 2C and S4A), and blocked AIS degradation (Figures 2D and S4B), redistribution of tau into the somatodendritic compartment (Figures 2E and S4C), and axonal degeneration throughout the brain (Figure 2F). Lastly, protective efficacy for cognition was assessed in the Barnes maze task of learning and memory. Daily treatment with CGP3466B (0.014 mg/kg IP), this time initiated 24 h after injury, protected mice from deficits in learning and memory (Figure 2G), without altering motor speed (Figures S4D and S4E) or body weight (Figure S4F).

**Figure 1. Neuronal tau acetylation after TBI induces axon initial segment degradation and pathologic tau mislocalization**

- (A) Quantified western blot shows increased ac-tau 6 h–2 weeks after TBI in cerebral cortex and hippocampus. Each group n = 3, \*\*p < 0.01, \*\*\*p < 0.001, \*\*\*\*p < 0.0001 versus sham-injury group, one-way ANOVA and Dunnett multiple comparisons test.
- (B) Quantified western blot shows increased ac-tau in neurons (NeuN<sup>+</sup>, GFAP<sup>-</sup>), but not glia (NeuN<sup>-</sup>, GFAP<sup>+</sup>), of the cerebral cortex, with greater tau expression in neurons. Each lane consists of pooled brain tissue from 3 animals, \*\*p < 0.01 versus sham-injury group, Student's t test.
- (C) Quantified western blot shows TBI intensity-dependent increase in ac-tau. Each group n = 3–4, \*\*p < 0.01, \*\*\*\*p < 0.0001 versus sham-injury group, one-way ANOVA and Dunnett multiple comparisons test. PSI, pounds per square inch of explosive pressure.
- (D) Quantified western blot shows reduced AIS proteins AnkG and  $\beta$ IV-spectrin after TBI, consistent with AIS degradation. Each group n = 3, \*p < 0.05, \*\*p < 0.01, \*\*\*p < 0.001 versus sham-injury group, one-way ANOVA and Dunnett multiple comparisons test.
- (E) Immunohistochemical staining for tau and the neuronal marker NeuN shows normal axonal localization of tau 2 weeks after sham-injury, and pathological tau mislocalization into the somatodendritic compartment 2 weeks after TBI (scale bar, 5  $\mu$ m). Images are representative of 3 animals per group.
- (F) Blast-injury induces increased cleaved caspase-3 levels and LDH release in TauKQ (mimicking acetylated lysine) overexpressing cells compared to TauWT (wild type) and TauKR (nonacetylatable tau mutant) transfected cells (\*\*p < 0.001, \*\*\*p < 0.0001 versus TauWT, TauKR transfected cells, one-way ANOVA, and Tukey's post hoc analysis).
- (G) TauKQ<sup>high</sup> mice have axonal degeneration in cerebral cortex, hippocampus, and hypothalamus, which is absent from nontransgenic littermates (\*p < 0.05, Student's t test).

See also Figures S1 and S2.



(legend on next page)

## Inhibiting p300/CBP acetyltransferase blocks injury-induced tau acetylation, neurodegeneration, and neurobehavioral impairment

Given the multiple mechanistic steps that follow injury-dependent S-nitrosylation of GAPDH to converge on elevating ac-tau, complementary therapeutic approaches were considered. Salsalate, a known inhibitor of rodent and human p300/CBP (Shirakawa et al., 2016), was tested first. Because salsalate has anti-inflammatory properties, a low dose that inhibited p300/CBP (Figures S5A–S5D) without blocking elevated levels of neuroinflammatory cytokines after injury (Figures S5E and S5F) was identified. Daily administration of this low non-anti-inflammatory dose of salsalate, beginning 24 h after TBI, reduced amounts of ac-tau in the brain without changing the total amount of tau protein (Figure 3A) or GAPDH S-nitrosylation (Figure S5G). This same low-dose salsalate treatment also preserved the AIS after injury, as evidenced by unchanged levels of AnkG and  $\beta$ V-spectrin (Figure 3B). Encouragingly, compared with sham-injured animals, low-dose salsalate preserved normal axonal localization of tau (Figures 3C and S5H) and protected mice from axonal degeneration (Figure 3D).

As a functional measure of protection, motor and cognitive function after injury were assessed (Figure 3E). Notably, daily low-dose, non-anti-inflammatory salsalate treatment initiated 24 h after injury preserved normal motor function in the foot slip assay (Figure 3E) and also protected mice from acquiring deficits in learning (Figures 3E and S6A) and memory (Figure 3E) in the Barnes maze task, without impacting body weight (Figure S6B) or motor speed (Figures S6C and S6D).

## Elevating NAD<sup>+</sup> enhances Sirt1 activity and blocks injury-induced tau acetylation, neurodegeneration, and neurobehavioral impairment

Next, we tested the complementary approach of increasing Sirt1-mediated tau deacetylation. Sirt1 activity is dependent on nicotinamide adenine dinucleotide (NAD<sup>+</sup>), and high expression of the Ube4b/nicotinamide mononucleotide adenylyltransferase 1 fusion protein in *Wld<sup>S</sup>* mice results in constitutively elevated NAD<sup>+</sup> levels that protect these animals from axonal degeneration and neurobehavioral impairment after brain injury (Pieper and

McKnight, 2018; Yin et al., 2016). Here, *Wld<sup>S</sup>* mice were also completely protected from injury-induced increases in ac-tau (Figure 4A) and AIS degradation throughout the brain (Figure 4B), which correlated with complete protection from tau mislocalization as well (Figures 4C and S5I).

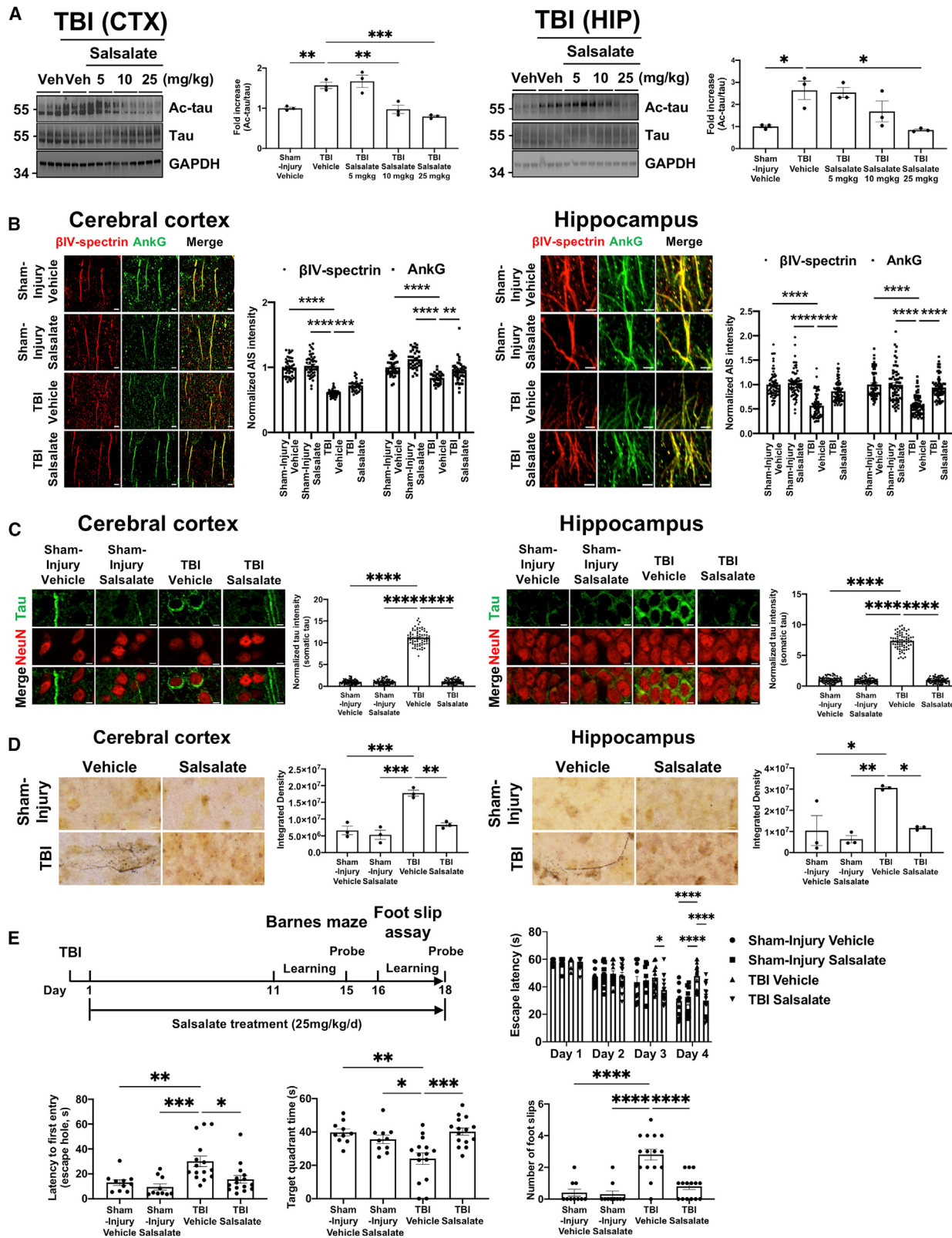
NAD<sup>+</sup> levels under conditions of neuronal stress can also be preserved by treatment with the aminopropyl carbazole P7C3-A20 (Pieper et al., 2010; Wang et al., 2014; Pieper and McKnight, 2018). Here, P7C3-A20, administered daily beginning 24 h after brain injury, preserved brain NAD<sup>+</sup> levels (Figure 5A) and prevented accumulation of ac-tau (Figure 5B). This correlated with protection from injury-induced AIS degradation (Figure 5C) and mislocalization of tau into the somatodendritic compartment (Figures 5D and S5J). Importantly, P7C3-A20-mediated protection was conferred without impacting upstream injury-induced S-nitrosylation of GAPDH (Figure 5E). All aspects of P7C3-A20-mediated protection were blocked by inhibiting Sirt1 with EX527 or inhibiting NAD<sup>+</sup> synthesis with FK866 (Figures 5A–5D). Thus, P7C3-A20-mediated preservation of otherwise depleted neuronal NAD<sup>+</sup> after brain injury promoted downstream Sirt1-mediated deacetylation of tau, which blocked neurodegeneration-inducing AIS degradation and tau mislocalization.

## Acetylated tau is a blood biomarker of traumatic brain injury-induced neurodegeneration in mice and humans

Because tau freely diffuses from brain to blood, we postulated that ac-tau might serve as a blood biomarker of post-TBI neurodegeneration. Western blot of immunoglobulin-depleted (because of its size overlap with tau) plasma revealed elevated levels of ac-tau in mouse plasma after TBI (Figure 6A). Specificity of plasma ac-tau was confirmed by using wild-type and tau knockout mice plasma samples with the same plasma immunoglobulin and albumin depletion strategy (Figure S6E) that has been previously established for assessment of rodent and human plasma tau under normal conditions and in AD or TBI (Sparks et al., 2012; Arun et al., 2013; Shekhar et al., 2016). Notably, the same protective therapies that reduced brain concentrations of ac-tau (treatment with CGP3466B, low-dose salsalate, or P7C3-A20) also decreased the concentration of ac-tau in plasma (Figures 6B–6E).

**Figure 2. SNO-GAPDH mediates the post-TBI p300/CBP acetyltransferase activation and Sirt1 deacetylase inhibition that leads to accumulated ac-tau, AIS degradation, tau mislocalization, neurodegeneration, and cognitive deficits**

- (A) Western blot and its quantification show significantly increased S-nitrosylation (SNO) of GAPDH and Sirt1 in cerebral cortex after TBI ( $n = 3$  per group, \* $p < 0.05$ , \*\* $p < 0.01$ , \*\*\* $p < 0.001$  versus sham-injury group, one-way ANOVA, and Dunnett multiple comparisons test). “Ascorbate (Asc) – negative control” shows specificity of signal in the SNO-resin-assisted capture technique.
  - (B) Western blot and its quantification show that treatment of CGP3466B inhibits S-nitrosylation of GAPDH and Sirt1 at 0.014 mg/kg. Each group  $n = 4$ , \*\* $p < 0.01$ , \*\*\* $p < 0.001$  versus TBI+vehicle group, one-way ANOVA and Tukey’s post hoc analysis. Asc + represents SNO, and Asc – represents control.
  - (C) Western blot and its quantification show that 0.014 mg/kg CGP3466B reduces ac-tau in cerebral cortex after TBI. Each group  $n = 4$ –7, \* $p < 0.05$ , \*\*\* $p < 0.001$  versus TBI+vehicle group, one-way ANOVA, and Tukey’s post hoc analysis.
  - (D) CGP3466B protects mice from post-TBI AIS degradation in the cerebral cortex (scale bar, 5  $\mu$ m).
  - (E) CGP3466B protects mice from post-TBI tau mislocalization (scale bar, 5  $\mu$ m). Lower magnification pictures of the field from which these pictures were derived are shown in Figure 4C.
  - (F) CGP3466B protects mice from post-TBI axonal degeneration, as evidenced by silver staining of degenerating axons (scale bar, 5  $\mu$ m).
  - In (D)–(F), each group  $n = 3$ –5, \* $p < 0.05$ , \*\* $p < 0.01$ , \*\*\* $p < 0.0001$  versus TBI+vehicle group, one-way ANOVA, and Tukey’s post hoc analysis.
  - (G) CGP3466B protects mice from post-TBI impaired cognition in both learning and memory phases of the Barnes maze task (\* $p < 0.05$ , \*\* $p < 0.01$ , \*\*\* $p < 0.001$ , \*\*\* $p < 0.0001$  versus TBI+vehicle group, repeated-measures two-way ANOVA (learning) and one-way ANOVA (memory) and Tukey’s post hoc analysis.
- See also Figures S3 and S4.



(legend on next page)

Next, to evaluate for clinical relevance in human patients, plasma ac-tau levels were evaluated from TBI patients admitted to a neuroscience intensive care unit of Memorial Herman Hospital-Texas Medical Center (Houston, TX) from December 2017 to April 2019 (Figure S6F; Table S1). In these patients, plasma neurofilament light chain (NfL), ubiquitin C-terminal hydrolase L1 (UCHL1), and glial fibrillary acidic protein (GFAP), but not phosphorylated tau (pTau181)/Tau, were increased relative to control samples (Figure 6F). Plasma ac-tau was also increased by ~50% within day 1 of admission compared to controls ( $p < 0.0001$ ) (Figure 6G) and remained consistently elevated across all time points (Figure S7A). Ac-tau levels showed no age- or gender-dependent differences (Figure S7B; for ac-tau female versus male 1.32 versus 1.64,  $p > 0.05$ ), and there was no tau seeding activity in human TBI versus control samples (Figure S7C). Lastly, specificity for elevated levels of plasma ac-tau in TBI was observed, relative to plasma samples from human patients with either subarachnoid hemorrhage (Figures 6H and S7D) or intracerebral hemorrhage (Figures 6I and S7E).

### Accumulation of ac-tau in the brains of patients with AD is significantly increased by a prior history of TBI

We next investigated whether increased ac-tau in AD would be further augmented by a previous history of TBI in people. Here, nine human frontal cortex brain specimens from the Northwestern University Alzheimer's Disease Research Center brain bank were analyzed. Cases were selected based on their cognitive status during life, history of TBI, and degree of Alzheimer's disease neuropathologic change (ADNC) at the time of brain autopsy (Montine et al., 2012; Hyman et al., 2012). There were three cases per study group, with ages ranging from 75–89 years old at the time of death. Group 1 consisted of normal controls with no cognitive impairment (NCI) and a maximum ADNC score of Low. Groups 2 and 3 consisted of subjects that had been diagnosed with dementia of the Alzheimer's type (DAT), with ADNC score of High. Group 2 had an additional history of TBI, whereas group 3 did not. Within group 2, TBI was required to have occurred prior to the onset of cognitive symptoms. Specifically, subject 1 in group 2 sustained a TBI from an unknown cause at age 23 with loss of consciousness (LOC). Subject 2 in group 2 sustained a TBI with LOC while playing football in high school and an additional TBI with LOC at age 72 after driving their tractor over a cliff. The duration of LOC for subject 1 or 2 was not known. Lastly, subject 3 in group 2 sustained a severe TBI of unknown cause at age 54 that resulted in coma for 4 days. Importantly, none of the selected cases had co-existing confounding lesions

involving the neocortex, such as neocortical Lewy body disease, and all cases were matched by age, sex, and post-mortem interval times (Table S2). Consistent with the hypothesis, ac-tau levels in AD patients in group 3 were significantly higher than ac-tau levels in group 1 NCI controls, and ac-tau levels in AD patients in group 2 with history of TBI were significantly higher than ac-tau levels in group 3 AD patients without a history of TBI (Figure 6J).

### NSAIDs that inhibit p300/CBP are associated with decreased incidence of clinically diagnosed TBI and AD in people

In addition to the NSAID salsalate, the related salicylate diflunisal also inhibits p300/CBP (Shirakawa et al., 2016). Although diflunisal has much lower blood-brain barrier penetration than salsalate, along the order of 1:100 (US Food and Drug Administration), it also inhibits p300/CBP acetyltransferase at much lower doses than what is typically administered for anti-inflammatory effect. Thus, we examined whether salsalate or diflunisal usage in people might be neuroprotective, relative to the commonly used NSAID aspirin that does not inhibit p300/CBP (Shirakawa et al., 2016). Notably, a recent randomized placebo-controlled trial in ~19,000 subjects showed that aspirin does not significantly reduce the incidence of dementia, minor cognitive impairment, or cognitive decline (Ryan et al., 2020).

The relationship between salsalate or diflunisal use and incidence of clinically diagnosed TBI or AD was investigated by analyzing 7.23 million United States (US) commercially insured individuals (MarketScan Medicare Supplemental database). Two cohort analyses were conducted to evaluate the predicted association, based on individual level of longitudinal patient data and pharmacoepidemiologic methods, as previously established (Cheng et al., 2018). The two cohorts included: (1) salsalate versus a matched aspirin population, and (2) diflunisal versus a matched aspirin population (Table S3). For each comparison, the un-stratified Kaplan-Meier curves and conducted propensity score (PS) stratified ( $n$  strata = 10) log-rank tests and a Cox regression model after adjusting age, race, sex, and disease comorbidities (including diabetes, hypertension, and coronary artery disease) were estimated using a PS-matching method. The International Classification of Diseases codes used to define the presence of each condition are listed in Table S4. After 6 years of follow-up, salsalate usage was associated with a significantly reduced risk of clinically diagnosed TBI (hazard ratio [HR] = 0.70, 95% confidence interval [CI] = 0.55–0.89,  $p < 0.001$ , Figure 7A) and AD (HR = 0.57, 95% CI = 0.42–0.77,

**Figure 3. Low-dose salsalate-mediated inhibition of p300/CBP acetyltransferase protects mice from post-TBI-induced elevated ac-tau, AIS degradation, tau mislocalization, neurodegeneration, and cognitive deficits**

(A) Low-dose salsalate dose-dependently reduces post-TBI elevations in ac-tau in the brain ( $n = 3$ , \* $p < 0.05$ , \*\* $p < 0.01$ , \*\*\* $p < 0.001$  versus TBI+vehicle group, one-way ANOVA, and Tukey's post hoc analysis).

(B) Low-dose salsalate protects mice from post-TBI AIS degradation (scale bar, 5  $\mu\text{m}$ ).

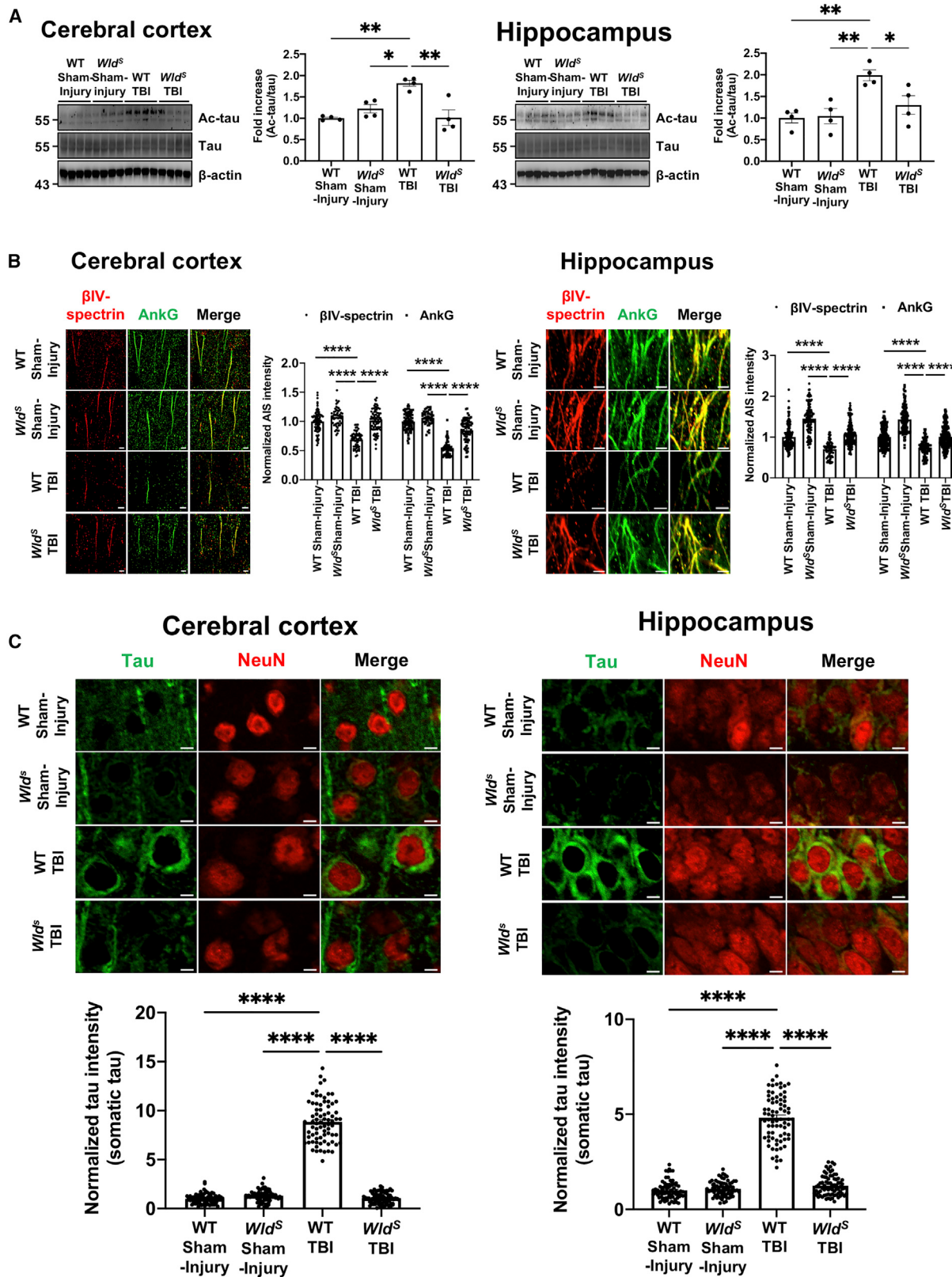
(C) Low-dose salsalate protects mice from post-TBI tau mislocalization (scale bar, 5  $\mu\text{m}$ ).

(D) Low-dose salsalate protects mice from post-TBI axonal degeneration (scale bar, 5  $\mu\text{m}$ ).

In (B)–(D), each group  $n = 3$ , \* $p < 0.05$ , \*\* $p < 0.01$ , \*\*\* $p < 0.001$ , \*\*\*\* $p < 0.0001$  versus TBI+vehicle group, one-way ANOVA and Tukey's post hoc analysis.

(E) Low-dose salsalate protects mice from post-TBI impairments in motor (foot slip assay) and cognitive (learning and memory in the Barnes maze) behavioral assays. (\* $p < 0.05$ , \*\* $p < 0.01$ , \*\*\* $p < 0.001$ , \*\*\*\* $p < 0.0001$  versus TBI+vehicle group, repeated-measures two-way ANOVA (learning) and one-way ANOVA (memory) and Tukey's post hoc analysis.

See also Figures S5 and S6.



(legend on next page)

$p < 0.001$ , Figure 7B), compared with a PS-matched aspirin cohort by Cox regression model. Strikingly, diflunisal usage was associated with an even greater reduced incidence of clinically diagnosed TBI (HR = 0.61, 95% CI = 0.43–0.86,  $p = 0.003$ , Figure 7A) and AD (HR = 0.17, 95% CI = 0.08–0.36,  $p < 0.001$ , Figure 7B), compared with a PS-matched aspirin cohort. The greater efficacy of diflunisal relative to salsalate correlates with the greater potency of diflunisal to inhibit p300/CBP. Lastly, to more specifically control for co-morbid factors associated with AD, additional subgroup analysis was performed by removing all subjects with diabetes, hypertension, and coronary artery disease. This confirmed that usage of either salsalate or diflunisal was associated with a reduced incidence of AD, with much stronger effect seen in patients prescribed diflunisal (Figure 7C).

Because diflunisal is an even more potent inhibitor of p300/CBP than salsalate, we postulated that this medicine might also inhibit the accumulation of ac-tau after brain injury in mice. After establishing that peripherally administered diflunisal dose-dependently crossed the blood-brain barrier in mice (Figure 7D), we orally administered this medicine to animals and then euthanized at the indicated times. After peripheral blood collection, animals were perfused with 1× PBS to remove blood in the brain vasculature. Total plasma and brain levels of diflunisal were evaluated by liquid chromatography-tandem mass spectrometry (LC-MS/MS) and then converted to free drug levels after measurement of binding in mouse plasma and brain. In line with previous observations of diflunisal levels in baboon cerebrospinal fluid (CSF) (Merck & Co.), there was relatively modest penetration of diflunisal into mouse brain. On average, across the two time points and three concentrations evaluated, the total diflunisal plasma to brain ratio was ~200:1. However, when free drug levels were calculated, the ratio decreased to only 55:1 because the fraction unbound in brain tissue was higher than in plasma ( $f_u_{\text{brain}} = 0.050 \pm 0.001$ ;  $f_u_{\text{plasma}} = 0.014 \pm 0.002$ ). Furthermore, when absolute concentrations were taken into account, total diflunisal brain levels reached ~3.9  $\mu\text{M}$  (972 ng/g), and free levels were 196 nM (49 ng/g) at the 50 mg/kg dose in mice. Total plasma levels at this dose ranged from 167–232  $\mu\text{g}/\text{mL}$  in mice, a concentration similar to mean peak levels of 190  $\pm$  33 mcg/mL observed in humans given 500 mg diflunisal twice daily for 11 days (Merck & Co.), confirming the physiologic relevance of the doses employed here. Therefore, the efficacy of daily diflunisal administration, beginning 24 h after TBI, to block the expected rise in neuronal ac-tau in mice was evaluated. As shown in Figure 7E, accumulation of ac-tau in cortical brain tissue progressively decreased with escalating doses of diflunisal. Moreover, this was reflected in dose-dependent decreases in blood ac-tau as well (Figure 7F), with tight correlation between plasma and brain levels of ac-tau (Figure 7G,  $R = 0.857$ ,  $p < 0.0001$ ).

## DISCUSSION

Taken together, our findings reveal critical cross-talk between S-nitrosylation and acetylation in neurons after brain injury, which converges on neuronal ac-tau. Although previous studies have reported phosphorylated tau in human TBI (Yang et al., 2017; Okamura et al., 2019; Gorgoraptis et al., 2019), these observations were beyond the first 24 h after injury, which was examined here. Importantly, independent analysis of the 24-h samples showed no increase in tau phosphorylation. Moreover, genetic *in vitro* and *in vivo* studies showed a direct neurotoxic effect of human ac-tau on neurons. Thus, our results support a critical role for tau acetylation in the acute period following brain injury, preceding any effects of tau phosphorylation. Future studies will focus on the interplay between tau acetylation and the myriad other pathological post-translational modifications of tau that have been reported, including phosphorylation and ubiquitination (Wesseling et al., 2020).

AD-like pathology in experimental systems had been linked previously to N-methyl-d-aspartic acid-mediated, neuronal nitric oxide synthase-dependent S-nitrosylation (Sen et al., 2018), and separately SNO-GAPDH had been implicated in modulating protein acetylation (Kornberg et al., 2010). However, understanding of the connection of protein S-nitrosylation to human-relevant *in vivo* models of neurodegeneration after brain injury was missing. The work here shows how this process mechanistically unfolds and how these insights form the basis of effective therapy. After injury, GAPDH S-nitrosylation leads to ac-tau accumulation and subsequent ac-tau-mediated pathology in neurons. Specifically, brain injury-induced SNO-GAPDH coordinately activates p300/CBP acetyltransferase and inhibits Sirt1 deacetylase to increase amounts of neuronal ac-tau. Drugging SNO-GAPDH with CGP3466B, or p300/CBP with low-dose salsalate or diflunisal, inhibits tau acetylation and downstream consequences of brain injury. It is important to recognize that these pharmacologic agents can have pleiotropic cellular effects, and thus we are unable to define how much of their neuroprotective effect is strictly due to reducing ac-tau. Given that all the neuroprotective agents examined in this study are also shown to reduce ac-tau *in vivo*, however, there is compelling support for a common mechanism. This viewpoint is further bolstered by the epidemiologic association of diflunisal and salsalate usage with decreased incidence of both AD and clinically diagnosed TBI in people. Moreover, the stronger effect of diflunisal compared to salsalate correlates with the greater potency with which diflunisal inhibits p300/CBP acetyltransferase. In addition, patient usage of the NSAID aspirin, which differs from the NSAIDs diflunisal and salsalate by not being able to inhibit p300/CBP acetyltransferase, did not show a protective effect. However, it is important to note that more patients took aspirin

### Figure 4. *Wld<sup>S</sup>* mice are protected from post-TBI-induced elevated ac-tau, AIS degradation, and tau mislocalization

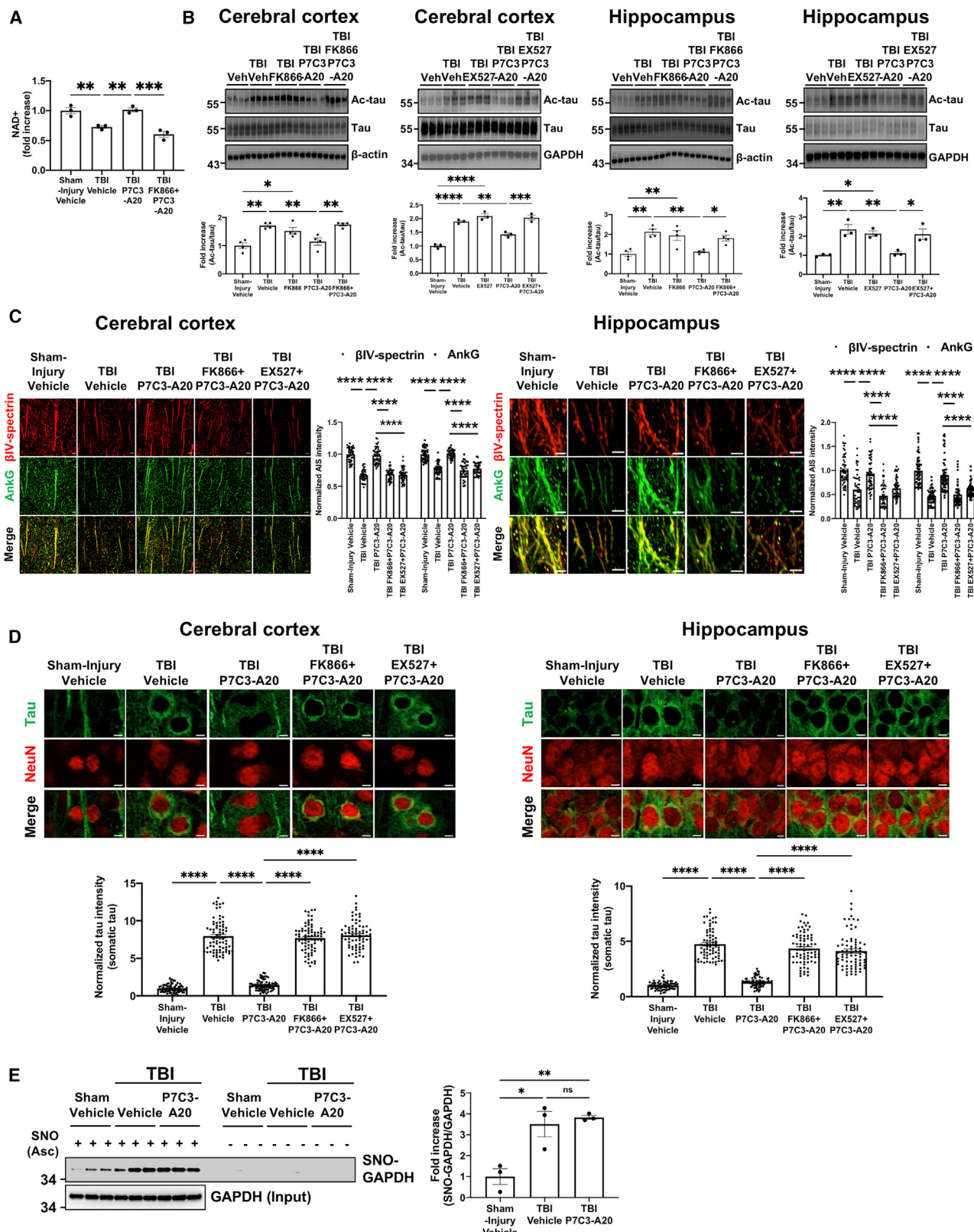
(A) *Wld<sup>S</sup>* mice are resistant to post-TBI elevations in ac-tau in the brain (for each group  $n = 4$ ,  $*p < 0.05$ ,  $**p < 0.01$  versus WT+TBI group, one-way ANOVA, and Tukey's post hoc analysis).

(B) *Wld<sup>S</sup>* mice are resistant to post-TBI AIS degradation (scale bar, 5  $\mu\text{m}$ ).

(C) *Wld<sup>S</sup>* mice are resistant to post-TBI tau mislocalization (scale bar, 5  $\mu\text{m}$ ).

In (B)–(C), each group  $n = 3$ ,  $***p < 0.0001$  versus WT+TBI group, one-way ANOVA, and Tukey's post hoc analysis.

See also Figure S5.



(legend on next page)

than diflunisal or salsalate, which is an unavoidable confounding factor of the patient population. In aggregate, the animal and human data presented here offer compelling support for a neuroprotective effect of reducing ac-tau, which supports further exploration of the potential protective efficacy of diflunisal or salsalate in patients with TBI or AD.

On the other side of the balance of acetylation, SNO-GAPDH-mediated inhibition of NAD<sup>+</sup>-dependent Sirt1 deacetylase is mediated by enzymatic S-nitrosylation of Sirt1, thereby preventing tau deacetylation. Maintaining Sirt1 activity through treatment with P7C3-A20, which preserves NAD<sup>+</sup> levels in injured neurons, also protected against the same deleterious outcomes after brain injury. Thus, multiple lines of evidence converge to show that reducing neuronal ac-tau is a successful therapeutic approach for treating TBI, whether that is through inhibiting acetylation with already existing drugs that could be repurposed for TBI, or through enhancing deacetylation through a drug to emerge from the P7C3 series of molecules. Other strategies to preserve NAD<sup>+</sup> after injury, such as pharmacologic inhibitors of the NAD<sup>+</sup> hydrolase SARM1, might be similarly effective (Pieper and McKnight, 2018; Hughes et al., 2021).

Both inhibition of tau acetylation and activation of tau deacetylation were observed following post-injury treatment with CGP34668, which selectively inhibits S-nitrosylation of GAPDH. CGP34668, also named “omigapil,” is an analog of the irreversible inhibitor of monoamine oxidase B known as deprenyl, which is employed to treat patients with Parkinson’s disease and depression. Notably, omigapil has recently shown safety in a Phase 1 clinical trial for patients with pediatric and adolescent congenital muscular dystrophy (CMD; NCT01805024). Abnormally frequent neurofibrillary tangles of tau in the cerebral cortex have been reported in several studies of CMD patients, and variations in tau have also been associated with CMD (Vermersch et al., 1996). Elucidation here of the downstream events in the brain following GAPDH-S-nitrosylation after brain injury may thus provide previously unanticipated strategies to preserve brain health in CMD patients. Because tau is also found in muscle fibers (Lübke et al., 1994), it is likewise possible that the signaling cascade and opportunities for therapeutic intervention that we have characterized here in the brain could apply to improving muscular health in patients with CMD.

Lastly, there is a tremendous unmet need for robust biomarkers that can establish whether a head injury has affected the brain, as well as stratify the severity and nature of the brain injury and objectively identify whether it is resolving. For example, a blood-based biomarker could overcome the limitations of current

neuropsychological tests for brain injury, and also help detect brain trauma that is masked by other injuries or symptoms. Rapid and accurate field diagnosis of brain injury is also critical for assuring that athletes and military personnel are not placed at risk for a second injury before they have fully recovered. While numerous cerebrospinal fluid biomarkers for brain injury have been proposed (Zetterberg and Blennow, 2016), collection of peripheral blood samples is considerably easier. However, the low concentration of potential biomarkers in peripheral blood can be technically limiting, and the concentration of brain proteins in the blood can vary as a function of integrity of the blood-brain barrier. Thus, a robust marker that freely diffuses across the blood-brain barrier from the brain into the blood, such as tau protein, is desired. Here, we have shown that ac-tau levels rapidly rise in the blood of both rodents and humans after brain injury, and that serum levels decline proportionally with protective treatments that target the underlying signaling cascade. Other proposed brain injury markers in the field include S100-B and GFAP, as blood biomarkers of astroglial injury (Mondello et al., 2018). However, neither of these is derived from degenerating neurons themselves, and S100-B is also robustly expressed in cells outside of the brain, such as adipocytes and chondrocytes (Olsson et al., 2011). Another candidate blood biomarker from brain injury is neuron-specific enolase (NSE), an enzyme involved in glycolytic energy metabolism (Mondello et al., 2018). However, the utility of NSE is limited because erythrocytes and platelets also contain high amounts of this enzyme (Tolan et al., 2013; Geisen et al., 2015), and elevated NSE is also associated with tumors, ischemic stroke, intracerebral hemorrhage, and seizures (Isgrò et al., 2015). Additional blood biomarkers for TBI include serum NfL and UCH-L1 (Shahim et al., 2020), although UCH-L1 is unable to distinguish mild TBI patients from those with orthopedic trauma (Posti et al., 2017). Taken together, the quest for blood biomarkers of TBI is an active and important area of investigation, and ac-tau may provide a uniquely valuable addition to the field. Importantly, ac-tau is mechanistically linked to both pathophysiology of neurodegeneration and a neuroprotective treatment strategy. Ac-tau levels in the blood correlate directly with its brain levels, and blood ac-tau appears to distinguish TBI-induced neurodegeneration from other forms of pathology, such as subarachnoid and intracerebral hemorrhage. Whether blood ac-tau levels correlate with the progression and severity of other forms of neurodegeneration, such as AD, remains to be investigated.

In summary, ac-tau is a previously unrecognized contributor to TBI pathophysiology. Tau acetylation sites after brain injury correspond to sites implicated in human AD, reflecting a shared

**Figure 5. P7C3-A20 treatment protects mice from post-TBI-induced elevated ac-tau, AIS degradation, and tau mislocalization**

- (A) P7C3-A20 treatment rescued normal NAD<sup>+</sup> levels after TBI, which was blocked by co-administration of FK866 (each group n = 3, \*p < 0.01, \*\*p < 0.001, one-way ANOVA and Tukey’s post hoc analysis).
- (B) P7C3-A20 treatment protects mice from post-TBI elevations in ac-tau in the brain (each group n = 3–4, \*p < 0.05, \*\*p < 0.01, \*\*\*p < 0.001, \*\*\*\*p < 0.0001, one-way ANOVA, and Tukey’s post hoc analysis). This protective effect is blocked by treatment with the NAMPT inhibitor FK866 or the Sirt1 Inhibitor EX527.
- (C) P7C3-A20 treatment protects mice from post-TBI AIS degradation (n = 3 per group, \*\*\*p < 0.0001, one-way ANOVA, and Tukey’s post hoc analysis). This protective effect is blocked by treatment with the NAMPT inhibitor FK866 or the Sirt1 Inhibitor EX527.
- (D) P7C3-A20 treatment protects mice from post-TBI tau mislocalization (each group n = 3, \*\*\*p < 0.0001, one-way ANOVA, and Tukey’s post hoc analysis, scale bar, 5 μm). This protective effect is blocked by treatment with the NAMPT inhibitor FK866 or the Sirt1 Inhibitor EX527.
- (E) SNO-GAPDH is not affected by P7C3-A20 (western blot, each group n = 3, \*p < 0.05, \*\*p < 0.01, one-way ANOVA and Tukey’s post hoc analysis). “Ascorbate (Asc) – negative control” shows specificity of signal in the SNO-resin-assisted capture technique.

See also Figure S5.

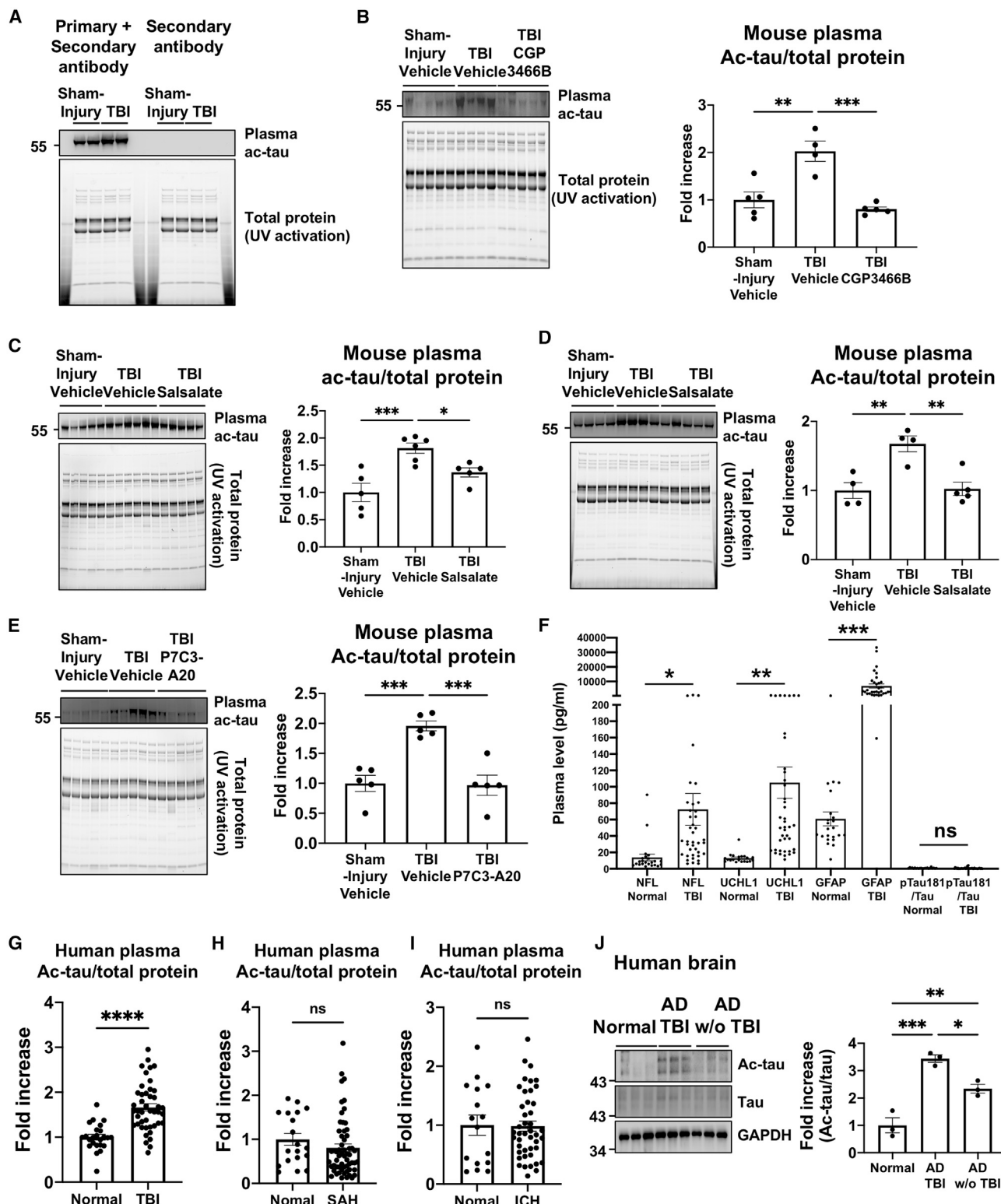


**Figure 6.** Elevated blood plasma ac-tau is a blood biomarker of TBI in mice and humans

(A) Western blot shows that TBI increases plasma ac-tau. Because tau and immunoglobulin G (IgG) have closely similar molecular weights, secondary antibody alone served as a control to ensure there was no cross reactivity with any residual IgG after IgG depletion.

(legend continued on next page)

mechanism of aberrant signaling that may serve as a pathophysiological mechanism for the increased risk of developing AD after TBI. This notion is supported by the observation of additionally increased ac-tau in the brains of patients with AD who also had a TBI prior to the onset of cognitive symptoms. Importantly, the presence of a small degree of baseline neuronal ac-tau in the uninjured and healthy brain prompts future investigation for a normal biological role of tau acetylation, with toxicity resulting when acetylation exceeds a threshold. At this time, our results establish that reducing ac-tau through multiple points of therapeutic intervention after brain injury offers a previously unanticipated neuroprotective strategy, and quantifying ac-tau in the blood provides biomarker of brain injury.

### Limitations of study

The utility of ac-tau as a biomarker of brain injury and neurodegeneration will need to be further established with more sophisticated measures of ac-tau and investigation of other neurodegenerative conditions. Another consideration is the presence of tau in muscle with respect to biomarker interpretation when there is comorbid muscular trauma with TBI. It is also important to note that although two sites of tau acetylation after TBI were examined here, there have been upwards of 20 tau acetylation sites identified in human tau in AD (Wesseling et al., 2020). Lastly, the retrospective human studies with diflunisal and salsalate in AD and TBI are correlative, and future prospective clinical trials are needed to confirm therapeutic efficacy.

### STAR★METHODS

Detailed methods are provided in the online version of this paper and include the following:

- KEY RESOURCES TABLE
- RESOURCE AVAILABILITY
  - Lead contact
  - Materials availability
  - Data and code availability
- EXPERIMENTAL MODEL AND SUBJECT DETAILS
  - Cell culture
  - Animals
  - Human subjects

- (B) Western blot and its quantification show that CGP3466B significantly reduced plasma ac-tau levels after TBI. Each group n = 4–5 with each lane representing a separated animal, \*\*p < 0.01, \*\*\*p < 0.001 versus TBI+vehicle group, one-way ANOVA, and Tukey's post hoc analysis.
- (C) Western blot and its quantification show that salsalate reduces plasma ac-tau levels. Each group n = 5–6 with each lane representing a separated animal, \*p < 0.05, \*\*p < 0.001 versus TBI+vehicle group, one-way ANOVA, and Tukey's post hoc analysis.
- (D) A repeat experiment in an independent cohort of animals confirmed the results shown in (C). Each lane represents a separate animal. For both (C) and (D), \*\*p < 0.01, TBI+vehicle group, one-way ANOVA, and Tukey's post hoc analysis.
- (E) Western blot and its quantification show that P7C3-A20 significantly reduced plasma ac-tau levels after TBI. Each group n = 5 with each lane representing a separated animal, \*\*\*p < 0.001 versus TBI+vehicle group, one-way ANOVA, and Tukey's post hoc analysis.
- (F) Plasma NfL, UCHL1, and GFAP, but not pTau181/Tau, levels are higher in TBI cohorts at 24 h after injury, compared to controls (\*p < 0.05, \*\*p < 0.01, \*\*\*p < 0.001).
- (G) The mean level of ac-tau was significantly higher in the TBI cohort at 24 h in comparison to the controls ( $1.8 \pm 0.58$  versus  $1.16 \pm 0.5$ , \*\*\*\*p < 0.0001).
- (H) The mean level of ac-tau in the subarachnoid hemorrhage (SAH) cohort at 24 h was no different from controls.
- (I) The mean level of ac-tau in the intracranial hemorrhage (ICH) cohort at 24 h was no different from controls.
- (J) Western blot and its quantification show that AD patients with TBI history have higher ac-tau levels than AD patients without TBI exposure (\*p < 0.05, \*\*p < 0.01, \*\*\*p < 0.001, one-way ANOVA, and Tukey's post hoc analysis).

See also Figures S6 and S7 and Tables S1 and S2.

### ● METHOD DETAILS

- In vitro traumatic brain injury
- In vivo multimodal traumatic brain injury
- In vivo controlled cortical impact traumatic brain injury
- In vivo acoustic blast overpressure traumatic brain injury
- Metabolomics
- Drug preparation and administration
- Behavioral analysis
- Western blotting
- Neuron and non-neuron isolation
- SNO-resin assisted capture (SNO-RAC)
- Postsynaptic density fractionation
- Immunohistochemistry
- Quantification of immunohistochemistry
- Quantitative real-time PCR
- NAD<sup>+</sup> measurement
- Preparation of plasma and albumin/immunoglobulin depletion
- Tau seed amplification assay (AD RT-QuIC)
- Quanterix
- Diflunisal pharmacokinetics
- Diflunisal protein binding
- Human plasma study
- Human brain study
- Pharmacoepidemiologic validation

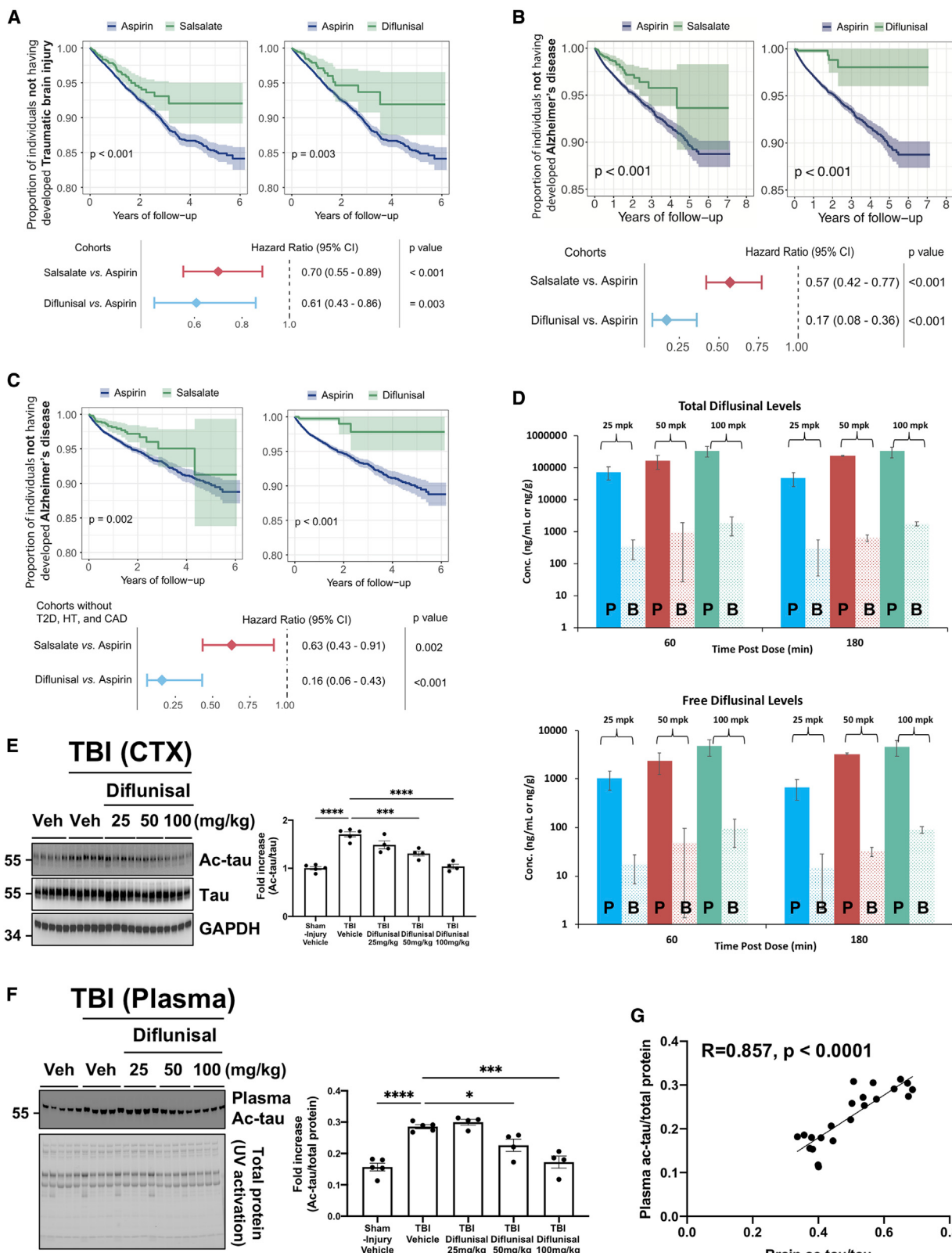
### ● QUANTIFICATION AND STATISTICAL ANALYSIS

### SUPPLEMENTAL INFORMATION

Supplemental information can be found online at <https://doi.org/10.1016/j.cell.2021.03.032>.

### ACKNOWLEDGMENTS

We thank those who provided blood and brain samples, Matthew N. Rasband for  $\beta$ IV-spectrin antibodies, Peter Davies for PHF1 (p-tau S396/S404) antibodies, Mikayla Huntley for tau seeding assay help, and Gloria Lee for providing brain tissue from tau knockout mice. Postmortem brain tissues were provided by the Neuropathology Core of Northwestern University (NIH P30 AG013854 24). We thank the Translational Therapeutics Core of the Cleveland Alzheimer's Disease Research Center (NIH/NIA 1 P30 AG062428-01) for assisting in the study with human postmortem brain tissues. The SV2 monoclonal antibody developed by K.M. Buckley was obtained from the



(legend on next page)

Developmental Studies Hybridoma Bank, created by the NICHD of the NIH, and maintained at The University of Iowa, Department of Biology (Iowa City, IA). This work was supported by a grant to A.A.P. from the Brockman Foundation. A.A.P. was also supported by Elizabeth Ring Mather and William Gwinn Mather Fund, S. Livingston Samuel Mather Trust, G.R. Lincoln Family Foundation, Wick Foundation, the Leonard Krieger Fund of the Cleveland Foundation, Gordon and Evie Safran, and Louis Stokes VA Medical Center resources and facilities. Acknowledgment is made to the donors of Alzheimer's Disease Research, a program of BrightFocus Foundation, for support of M.-K.S. in this research (A2019551F). A.A.P., M.K.J., J.D.R., and J.S.S. are supported by Project 19PABH134580006-AHA/Allen Initiative in Brain Health and Cognitive Impairment. E.V.-R. was supported by Free Radical and Radiation Biology, University of Iowa (T32 CA078586). F.C. and A.A.P. are supported together by NIA/NIH (RO1AG066707) and also the Translational Therapeutic Core of the Cleveland Alzheimer's Disease Research Center (NIH/NIA 1 P30 AGO62428-01), which assisted in the study of human postmortem brain tissue and longitudinal analysis of patient data. D.J.L. was supported by The Miami Project to Cure Paralysis and NIH/NINDS (NS098740). S.J.F. and M.T.P. were supported by VA BLR&D MERIT Award (2 101 BXOO2439-04A1) and Research Career Scientist Awards from Department of Veterans Affairs, with resources of VA Western NY Healthcare System (Buffalo, NY), and Atlanta VA Medical Center (Decatur, GA). S.J.F. was supported by Clinical and Translational Science Award (UL1TR001412) to University of Buffalo from National Center for Advancing Translational Sciences (NCATS/NIH). R.S.A. was supported by Career Development Award (CDA-2 RX002928) from Department of Veterans Affairs. T.G. was supported by NIA/NIH (RO1AG062566). M.E.F. was supported by NIA/NIH (K08AG065463).

#### AUTHOR CONTRIBUTIONS

M.-K.S., E.V.-R., and A.A.P. designed experiments and interpreted data. M.K.J. and J.D.R. assisted with experimental design and data interpretation. M.-K.S., E.V.-R., Y.K., M.D., K.C., K.F., C.C.-P., S.B., E.M., and M.N. conducted experiments. R.S.A., C.T.M., S.R.R., M.T.P., L.A.S., and S.J.F. supplied brain tissue from acoustic blast overpressure injury. D.J.L. supplied brain tissue from controlled cortical impact injury. C.W. and L.G. provided antibodies to acetylated tau. T.E.T. provided transgenic mouse brain tissue and SV2 immunohistochemical analysis. J.P.J.S., G.L.T., H.A., L.D.M., R.S.K., and H.A.C. collected plasma from human subjects. D.S. and J.S.S. assisted with S-nitrosylation experiments. A.K. and S.B. conducted tau seeding experiments. P.Z., Y.H., C.-W.C., L.L., and F.C. conducted analysis of NSAID usage and incidence of Alzheimer's disease. F.O., J.A.K., and N.S.W. conducted diflunisal pharmacokinetic studies. M.E.F. and T.G. assisted in study of human postmortem brain tissue. V.E.W. assisted in analysis of human plasma sam-

ples. A.A.P., M.-K.S., E.V.-R., M.K.J., J.S.S., and J.D.R. wrote the manuscript. All authors reviewed and approved the manuscript.

#### DECLARATION OF INTERESTS

A.A.P. is an inventor on patents related to P7C3. L.G. is a founder of Aeton Therapeutics. No other authors declare competing interests.

Received: October 5, 2020

Revised: January 21, 2021

Accepted: March 15, 2021

Published: April 13, 2021

#### REFERENCES

- Allen, R.S., Motz, C.T., Feola, A., Chesler, K.C., Haider, R., Ramachandra Rao, S., Skelton, L.A., Fliesler, S.J., and Pardue, M.T. (2018). Long-term functional and structural consequences of primary blast overpressure to the eye. *J. Neurotrauma* 35, 2104–2116.
- Arun, P., Abu-Taleb, R., Oguntayo, S., Tanaka, M., Wang, Y., Valiyaveettil, M., Long, J.B., Zhang, Y., and Nambiar, M.P. (2013). Distinct patterns of expression of traumatic brain injury biomarkers after blast exposure: role of compromised cell membrane integrity. *Neurosci. Lett.* 552, 87–91.
- Bolós, M., Llorens-Martín, M., Perea, J.R., Jurado-Arjona, J., Rábano, A., Hernández, F., and Avila, J. (2017). Absence of CX3CR1 impairs the internalization of Tau by microglia. *Mol. Neurodegener.* 12, 59.
- Cao, G., Xing, J., Xiao, X., Liou, A.K.F., Gao, Y., Yin, X.-M., Clark, R.S.B., Graham, S.H., and Chen, J. (2007). Critical role of calpain I in mitochondrial release of apoptosis-inducing factor in ischemic neuronal injury. *J. Neurosci.* 27, 9278–9293.
- Centers for Disease Control and Prevention (2015). Report to Congress on Traumatic Brain Injury in the United States: Epidemiology and Rehabilitation (National Center for Injury Prevention and Control: Division of Unintentional Injury Prevention).
- Cheng, F., Desai, R.J., Handy, D.E., Wang, R., Schneeweiss, S., Barabási, A.-L., and Loscalzo, J. (2018). Network-based approach to prediction and population-based validation of *in silico* drug repurposing. *Nat. Commun.* 9, 2691.
- Cohen, T.J., Guo, J.L., Hurtado, D.E., Kwong, L.K., Mills, I.P., Trojanowski, J.Q., and Lee, V.M. (2011). The acetylation of tau inhibits its function and promotes pathological tau aggregation. *Nat. Commun.* 2, 252.

#### Figure 7. Diflunisal usage is associated with decreased incidence of TBI and AD in people and with inhibition of ac-tau after TBI in mice

(A) Longitudinal analyses reveal that salsalate and diflunisal usages reduce risk of traumatic brain injury (TBI) in all patient data from the IBM MarketScan Medicare Supplemental Database. The un-stratified Kaplan-Meier curves, conducted propensity score stratified (n strata = 10) log-rank test and Cox model, and hazard ratio and 95% confidence interval for two cohort studies, were illustrated for both (A) and (B). Two cohort studies were conducted including: (1) salsalate users and aspirin users, and (2) diflunisal users and aspirin users. Using propensity score stratified survival analyses by adjusting the initiation time of drugs, enrollment history, age and gender, and disease comorbidities (diabetes, or hypertension, or coronary artery disease). Propensity score stratified Cox-proportional hazards models were used to conduct statistical inference for the hazard ratios.

(B) Longitudinal analyses reveal that salsalate and diflunisal usage in the same group as (A) is also associated with reduced incidence of AD in people.

(C) Subgroup analyses after excluding patients with type 2 diabetes, hypertension, or coronary artery disease (known risk factors for AD) further confirms that salsalate or diflunisal usage is associated with decreased incidence of AD.

(D) LC-MS/MS analysis shows modest penetration of diflunisal into mouse brain but the plasma:brain ratio is decreased when protein binding is taken into account and free drug levels are compared. Drug levels in plasma and brain were determined by LC-MS/MS analysis after mice were administered three different concentrations of diflunisal and euthanized 60 or 180 min later, followed by collection of blood and perfusion with saline, prior to harvesting brain tissue. Rapid equilibrium dialysis was used to determine binding of diflunisal in mouse plasma and brain homogenate. "P" and "B" denote plasma and brain, respectively.

(E) Diflunisal treatment dose-dependently reduces post-TBI elevations in ac-tau in the brain. Each group n = 4–5, \*\*\*p < 0.001, \*\*\*p < 0.0001 versus TBI+vehicle group, one-way ANOVA, and Tukey's post hoc analysis.

(F) Western blot and its quantification show that diflunisal dose-dependently reduced plasma ac-tau levels after TBI. Each group n = 4–5 with each lane representing a separate animal, \*p < 0.05, \*\*p < 0.01, \*\*\*p < 0.0001 versus TBI+vehicle group, one-way ANOVA, and Tukey's post hoc analysis.

(G) There is a significant correlation between brain and plasma ac-tau levels after brain injury (data from C and D; R = 0.857, p < 0.0001).

See also Tables S3 and S4.

- Cook, C., Carlonmagno, Y., Gendron, T.F., Dunmore, J., Scheffel, K., Stetler, C., Davis, M., Dickson, D., Jarpe, M., DeTure, M., and Petrucelli, L. (2014). Acetylation of the KXGS motifs in tau is a critical determinant in modulation of tau aggregation and clearance. *Hum. Mol. Genet.* 23, 104–116.
- Dutca, L.M., Stasheff, S.F., Hedberg-Buenz, A., Rudd, D.S., Batra, N., Blodi, F.R., Yorek, M.S., Yin, T., Shankar, M., Herlein, J.A., et al. (2014). Early detection of subclinical visual damage after blast-mediated TBI enables prevention of chronic visual deficit by treatment with P7C3-S243. *Invest. Ophthalmol. Vis. Sci.* 55, 8330–8341.
- Evans, D.B., Rank, K.B., Bhattacharya, K., Thomsen, D.R., Gurney, M.E., and Sharma, S.K. (2000). Tau phosphorylation at serine 396 and serine 404 by human recombinant tau protein kinase II inhibits tau's ability to promote microtubule assembly. *J. Biol. Chem.* 275, 24977–24983.
- Forrester, M.T., Thompson, J.W., Foster, M.W., Nogueira, L., Moseley, M.A., and Stamler, J.S. (2009). Proteomic analysis of S-nitrosylation and denitrosylation by resin-assisted capture. *Nat. Biotechnol.* 27, 557–559.
- Geisen, U., Benk, C., Beyersdorf, F., Klemm, R., Trummer, G., Özbek, B., Kern, F., and Heilmann, C. (2015). Neuron-specific enolase correlates to laboratory markers of haemolysis in patients on long-term circulatory support. *Eur. J. Cardiothorac. Surg.* 48, 416–420, discussion 420.
- Gorgoraptis, N., Li, L.M., Whittington, A., Zimmerman, K.A., Maclean, L.M., McLeod, C., Ross, E., Heslegrave, A., Zetterberg, H., Passchier, J., et al. (2019). In vivo detection of cerebral tau pathology in long-term survivors of traumatic brain injury. *Sci. Transl. Med.* 11, eaaw1993.
- Hara, M.R., and Snyder, S.H. (2006). Nitric oxide-GAPDH-Siah: a novel cell death cascade. *Cell. Mol. Neurobiol.* 26, 527–538.
- Hughes, R.O., Bosanac, T., Mao, X., Engber, T.M., DiAntonio, A., Milbrandt, J., Devraj, R., and Krauss, R. (2021). Small molecule SARM1 inhibitors recapitulate the SARM1<sup>−/−</sup> phenotype and allow recovery of a metastable pool of axons fated to degenerate. *Cell Rep.* 34, 108588.
- Hyman, B.T., Phelps, C.H., Beach, T.G., Bigio, E.H., Cairns, N.J., Carrillo, M.C., Dickson, D.W., Duyckaerts, C., Frosch, M.P., Masliah, E., et al. (2012). National Institute on Aging-Alzheimer's Association guidelines for the neuropathologic assessment of Alzheimer's disease. *Alzheimers Dement.* 8, 1–13.
- Irwin, D.J., Cohen, T.J., Grossman, M., Arnold, S.E., Xie, S.X., Lee, V.M., and Trojanowski, J.Q. (2012). Acetylated tau, a novel pathological signature in Alzheimer's disease and other tauopathies. *Brain* 135, 807–818.
- Isgrò, M.A., Bottini, P., and Scatena, R. (2015). Neuron-specific enolase as a biomarker: biochemical and clinical aspects. *Adv. Exp. Med. Biol.* 867, 125–143.
- Johnson, V.E., Stewart, W., and Smith, D.H. (2010). Traumatic brain injury and amyloid-β pathology: a link to Alzheimer's disease? *Nat. Rev. Neurosci.* 11, 361–370.
- Kornberg, M.D., Sen, N., Hara, M.R., Juluri, K.R., Nguyen, J.V.K., Snowman, A.M., Law, L., Hester, L.D., and Snyder, S.H. (2010). GAPDH mediates nitrosylation of nuclear proteins. *Nat. Cell Biol.* 12, 1094–1100.
- Kraus, A., Saijo, E., Metrick, M.A., 2nd, Newell, K., Sigurdson, C.J., Zanusso, G., Ghetti, B., and Caughey, B. (2019). Seeding selectivity and ultrasensitive detection of tau aggregate conformers of Alzheimer disease. *Acta Neuropathol.* 137, 585–598.
- Kristian, T. (2010). Isolation of Mitochondria from the CNS. *Curr. Protoc. Neurosci. Chapter 7, Unit 7.22.*
- Li, Y., Li, Y., Li, X., Zhang, S., Zhao, J., Zhu, X., and Tian, G. (2017). Head injury as a risk factor for dementia and Alzheimer's disease: a systematic review and meta-analysis of 32 observational studies. *PLoS ONE* 12, e0169650.
- LoCoco, P.M., Risinger, A.L., Smith, H.R., Chavera, T.S., Berg, K.A., and Clarke, W.P. (2017). Pharmacological augmentation of nicotinamide phosphoribosyltransferase (NAMPT) protects against paclitaxel-induced peripheral neuropathy. *eLife* 6, e29626.
- Lübke, U., Six, J., Villanova, M., Boons, J., Vandermeeren, M., Ceuterick, C., Cras, P., and Martin, J.J. (1994). Microtubule-associated protein tau epitopes are present in fiber lesions in diverse muscle disorders. *Am. J. Pathol.* 145, 175–188.
- Lucke-Wold, B., Seidel, K., Udo, R., Omalu, B., Ornstein, M., Nolan, R., Rosen, C., and Ross, J. (2017). Role of tau acetylation in Alzheimer's disease and chronic traumatic encephalopathy: the way forward for successful treatment. *J. Neurol. Neurosurg. 4*, 140.
- Ma, V.Y., Chan, L., and Carruthers, K.J. (2014). Incidence, prevalence, costs, and impact on disability of common conditions requiring rehabilitation in the United States: stroke, spinal cord injury, traumatic brain injury, multiple sclerosis, osteoarthritis, rheumatoid arthritis, limb loss, and back pain. *Arch. Phys. Med. Rehabil.* 95, 986–995.e1.
- Min, S.-W., Cho, S.-H., Zhou, Y., Schroeder, S., Haroutunian, V., Seeley, W.W., Huang, E.J., Shen, Y., Masliah, E., Mukherjee, C., et al. (2010). Acetylation of tau inhibits its degradation and contributes to tauopathy. *Neuron* 67, 953–966.
- Mondello, S., Sorinola, A., Czeiter, E., Vamos, Z., Amrein, K., Synnot, A., Donoghue, E., Sandor, J., Wang, K.K.W., Diaz-Arrastia, R., et al. (2018). Blood-based protein biomarkers for the management of traumatic brain injuries in adults presenting to emergency departments with mild brain injury: a living systematic review and meta-analysis. *J. Neurotrauma.* Published online July 2, 2018. <https://doi.org/10.1089/neu.2017.5182>.
- Montine, T.J., Phelps, C.H., Beach, T.G., Bigio, E.H., Cairns, N.J., Dickson, D.W., Duyckaerts, C., Frosch, M.P., Masliah, E., Mirra, S.S., et al.; National Institute on Aging; Alzheimer's Association (2012). National Institute on Aging-Alzheimer's Association guidelines for the neuropathologic assessment of Alzheimer's disease: a practical approach. *Acta Neuropathol.* 123, 1–11.
- Nakamura, T., and Lipton, S.A. (2020). Nitric oxide-dependent protein post-translational modifications impair mitochondrial function and metabolism to contribute to neurodegenerative diseases. *Antioxid. Redox Signal.* 32, 817–833.
- Neddens, J., Temmel, M., Flunkert, S., Kerschbaumer, B., Hoeller, C., Loeffler, T., Niederkofler, V., Daum, G., Attems, J., and Hutter-Paier, B. (2018). Phosphorylation of different tau sites during progression of Alzheimer's disease. *Acta Neuropathol. Commun.* 6, 52.
- Newman, A.J., Hayes, S.H., Rao, A.S., Allman, B.L., Manohar, S., Ding, D., Stolzberg, D., Lobatinas, E., Mollendorf, J.C., and Salvi, R. (2015). Low-cost blast wave generator for studies of hearing loss and brain injury: blast wave effects in closed spaces. *J. Neurosci. Methods* 242, 82–92.
- Okamura, Y., Kawakami, I., Watanabe, K., Oshima, K., Niizato, K., Ikeda, K., Akiyama, H., and Hasegawa, M. (2019). Tau progression in single severe frontal traumatic brain injury in human brains. *J. Neurol. Sci.* 407, 116495.
- Olsson, B., Zetterberg, H., Hampel, H., and Blennow, K. (2011). Biomarker-based dissection of neurodegenerative diseases. *Prog. Neurobiol.* 95, 520–534.
- Orešić, M., Posti, J.P., Kamstrup-Nielsen, M.H., Takala, R.S.K., Lingsma, H.F., Mattila, I., Jäntti, S., Katila, A.J., Carpenter, K.L.H., Ala-Seppälä, H., et al. (2016). Human serum metabolites associate with severity and patient outcomes in traumatic brain injury. *EBioMedicine* 12, 118–126.
- Perea, J.R., López, E., Díez-Ballesteros, J.C., Ávila, J., Hernández, F., and Bóilo, M. (2019). Extracellular monomeric tau is internalized by astrocytes. *Front. Neurosci.* 13, 442.
- Pieper, A.A., and McKnight, S.L. (2018). Benefits of enhancing nicotinamide adenine dinucleotide levels in damaged or diseased nerve cells. *Cold Spring Harb. Symp. Quant. Biol.* 83, 207–217.
- Pieper, A.A., Xie, S., Capota, E., Estill, S.J., Zhong, J., Long, J.M., Becker, G.L., Huntington, P., Goldman, S.E., Shen, C.-H., et al. (2010). Discovery of a pro-neurogenic, neuroprotective chemical. *Cell* 142, 39–51.
- Posti, J.P., Hossain, I., Takala, R.S.K., Liedes, H., Newcombe, V., Outtrim, J., Katila, A.J., Frantzén, J., Ala-Seppälä, H., Coles, J.P., et al. (2017). Glial fibrillary acidic protein and ubiquitin C-terminal hydrolase-L1 are not specific biomarkers for mild CT-negative traumatic brain injury. *J. Neurotrauma* 34, 1427–1438.
- Ruifrok, A.C., and Johnston, D.A. (2001). Quantification of histochemical staining by color deconvolution. *Anal. Quant. Cytol. Histol.* 23, 291–299.
- Ryan, J., Storey, E., Murray, A.M., Woods, R.L., Wolfe, R., Reid, C.M., Nelson, M.R., Chong, T.T.J., Williamson, J.D., Ward, S.A., et al.; ASPREE Investigator

- Group (2020). Randomized placebo-controlled trial of the effects of aspirin on dementia and cognitive decline. *Neurology* 95, e320–e331.
- Schafer, D.P., Jha, S., Liu, F., Akella, T., McCullough, L.D., and Rasband, M.N. (2009). Disruption of the axon initial segment cytoskeleton is a new mechanism for neuronal injury. *J. Neurosci.* 29, 13242–13254.
- Schmittgen, T.D., and Livak, K.J. (2008). Analyzing real-time PCR data by the comparative C(T) method. *Nat. Protoc.* 3, 1101–1108.
- Sen, T., Saha, P., and Sen, N. (2018). Nitrosylation of GAPDH augments pathological tau acetylation upon exposure to amyloid- $\beta$ . *Sci. Signal.* 11, eaao6765.
- Shahim, P., Politis, A., van der Merwe, A., Moore, B., Ekanayake, V., Lippa, S.M., Chou, Y.-Y., Pham, D.L., Butman, J.A., Diaz-Arrastia, R., et al. (2020). Time course and diagnostic utility of NFL, tau, GFAP, and UCH-L1 in subacute and chronic TBI. *Neurology* 95, e623–e636.
- Shekhar, S., Kumar, R., Rai, N., Kumar, V., Singh, K., Upadhyay, A.D., Tripathi, M., Dwivedi, S., Dey, A.B., and Dey, S. (2016). Estimation of tau and phosphorylated tau181 in serum of Alzheimer's disease and mild cognitive impairment patients. *PLoS ONE* 11, e0159099.
- Shin, M.-K., Vázquez-Rosa, E., Cintrón-Pérez, C., Riegel, A., Harper, M.M., Ritzel, D., and Pieper, A.A. (2021). Characterization of the jet-flow overpressure model of traumatic brain injury in mice. *Neurotrauma Rep.* 2, 1–13.
- Shirakawa, K., Wang, L., Man, N., Maksimoska, J., Sorum, A.W., Lim, H.W., Lee, I.S., Shimazu, T., Newman, J.C., Schröder, S., et al. (2016). Salicylate, diflunisal and their metabolites inhibit CBP/p300 and exhibit anticancer activity. *eLife* 5, e11156.
- Sohn, P.D., Tracy, T.E., Son, H.-I., Zhou, Y., Leite, R.E.P., Miller, B.L., Seeley, W.W., Grinberg, L.T., and Gan, L. (2016). Acetylated tau destabilizes the cytoskeleton in the axon initial segment and is mislocalized to the somatodendritic compartment. *Mol. Neurodegener.* 11, 47.
- Sparks, D.L., Kryscio, R.J., Sabbagh, M.N., Ziolkowski, C., Lin, Y., Sparks, L.M., Liebsack, C., and Johnson-Traver, S. (2012). Tau is reduced in AD plasma and validation of employed ELISA methods. *Am. J. Neurodegener. Dis.* 1, 99–106.
- Tolan, N.V., Vidal-Folch, N., Algeciras-Schimrich, A., Singh, R.J., and Grebe, S.K. (2013). Individualized correction of neuron-specific enolase (NSE) measurement in hemolyzed serum samples. *Clin. Chim. Acta* 424, 216–221.
- Tracy, T.E., Sohn, P.D., Minami, S.S., Wang, C., Min, S.-W., Li, Y., Zhou, Y., Le, D., Lo, I., Ponnusamy, R., et al. (2016). Acetylated tau obstructs KIBRA-mediated signaling in synaptic plasticity and promotes tauopathy-related memory loss. *Neuron* 90, 245–260.
- Uehara, T., Nakamura, T., Yao, D., Shi, Z.-Q., Gu, Z., Ma, Y., Masliah, E., Nomura, Y., and Lipton, S.A. (2006). S-nitrosylated protein-disulphide isomerase links protein misfolding to neurodegeneration. *Nature* 441, 513–517.
- US Food and Drug Administration. Manufacturer data sheet 9676203, Dolobid (Diflunisal). Merck & Co, Inc. [https://www.accessdata.fda.gov/drugsatfda\\_docs/label/2007/018445s058lbl.pdf](https://www.accessdata.fda.gov/drugsatfda_docs/label/2007/018445s058lbl.pdf).
- Vázquez-Rosa, E., Watson, M.R., Sahn, J.J., Hodges, T.R., Schroeder, R.E., Cintrón-Pérez, C.J., Shin, M.K., Yin, T.C., Emery, J.L., Martin, S.F., et al. (2019). Neuroprotective efficacy of a sigma 2 receptor/TMEM97 modulator (DKR-1677) after traumatic brain injury. *ACS Chem. Neurosci.* 10, 1595–1602.
- Vázquez-Rosa, E., Shin, M.-K., Dhar, M., Chaubey, K., Cintrón-Pérez, C.J., Tang, X., Liao, X., Miller, E., Koh, Y., Barker, S., et al. (2020). P7C3-A20 treatment one year after TBI in mice repairs the blood-brain barrier, arrests chronic neurodegeneration, and restores cognition. *Proc. Natl. Acad. Sci. USA* 117, 27667–27675.
- Vermersch, P., Sergeant, N., Ruchoux, M.M., Hofmann-Radvanyi, H., Wattez, A., Petit, H., Dwailly, P., and Delacourte, A. (1996). Specific tau variants in the brains of patients with myotonic dystrophy. *Neurology* 47, 711–717.
- Waldmeier, P.C., Spooren, W.P., and Hengerer, B. (2000). CGP 3466 protects dopaminergic neurons in lesion models of Parkinson's disease. *Naunyn Schmiedebergs Arch. Pharmacol.* 362, 526–537.
- Wang, G., Han, T., Nijhawan, D., Theodoropoulos, P., Naidoo, J., Yadavalli, S., Mirzaei, H., Pieper, A.A., Ready, J.M., and McKnight, S.L. (2014). P7C3 neuroprotective chemicals function by activating the rate-limiting enzyme in NAD salvage. *Cell* 158, 1324–1334.
- Wattiez, A.-S., Castonguay, W.C., Gaul, O.J., Waite, J.S., Schmidt, C.M., Reis, A., Rea, B.J., Sowers, L.P., Cintrón-Pérez, C., Vázquez-Rosa, E., et al. (2021). Different forms of traumatic brain injury cause different tactile hypersensitivity profiles. *Pain* 162, 1163–1175.
- Wesseling, H., Mair, W., Kumar, M., Schlaffner, C.N., Tang, S., Beerepoot, P., Fatou, B., Guise, A.J., Cheng, L., Takeda, S., et al. (2020). Tau PTM profiles identify patient heterogeneity and stages of Alzheimer's disease. *Cell* 183, 1699–1713.e13.
- Yang, W.-J., Chen, W., Chen, L., Guo, Y.-J., Zeng, J.-S., Li, G.-Y., and Tong, W.-S. (2017). Involvement of tau phosphorylation in traumatic brain injury patients. *Acta Neurol. Scand.* 135, 622–627.
- Yin, T.C., Britt, J.K., De Jesús-Cortés, H., Lu, Y., Genova, R.M., Khan, M.Z., Voorhees, J.R., Shao, J., Katzman, A.C., Huntington, P.J., et al. (2014). P7C3 neuroprotective chemicals block axonal degeneration and preserve function after traumatic brain injury. *Cell Rep.* 8, 1731–1740.
- Yin, T.C., Voorhees, J.R., Genova, R.M., Davis, K.C., Madison, A.M., Britt, J.K., Cintrón-Pérez, C.J., McDaniel, L., Harper, M.M., and Pieper, A.A. (2016). Acute axonal degeneration drives development of cognitive, motor, and visual deficits after blast-mediated traumatic brain injury in mice. *eNeuro* 3, ENEURO.0220-16.2016.
- Zetterberg, H., and Blennow, K. (2016). Fluid biomarkers for mild traumatic brain injury and related conditions. *Nat. Rev. Neurol.* 12, 563–574.

## STAR★METHODS

## KEY RESOURCES TABLE

REAGENT or RESOURCE	SOURCE	IDENTIFIER
<b>Antibodies</b>		
Rabbit polyclonal anti-ac-tau	Li Gan	N/A
Mouse monoclonal anti-tau	Abcam	Cat#ab80579; RRID:AB_1603723
Mouse monoclonal anti-tau	Thermo Fisher Scientific	Cat# 13-6400; RRID:AB_86533
Mouse monoclonal anti-β-actin	Santa Cruz Biotechnology	Cat# sc-47778; RRID:AB_626632
Mouse monoclonal anti-GAPDH	Millipore	Cat# MAB374; RRID:AB_2107445
Mouse monoclonal anti-NeuN	Millipore	Cat# MAB377; RRID:AB_2298772
Mouse monoclonal anti-GFAP	Thermo Fisher Scientific	Cat# MA5-12023; RRID:AB_10984338
Mouse monoclonal anti-SIRT1	Abcam	Cat# ab110304; RRID:AB_10864359
Rabbit polyclonal anti-p300	Santa Cruz Biotechnology	Cat# sc-584; RRID:AB_2293429
Rabbit monoclonal anti-CBP	Cell Signaling Technology	Cat# 7389; RRID:AB_2616020
Rabbit polyclonal anti-Histone H2AK5	Abcam	Cat# ab1764; RRID:AB_10563138
Rabbit monoclonal anti-Histone H2A	Cell Signaling Technology	Cat# 12349; RRID:AB_2687875
Rabbit polyclonal anti-Histone H3K18	Abcam	Cat# ab1191; RRID:AB_298692
Rabbit monoclonal anti-Histone H3	Cell Signaling Technology	Cat# 4499; RRID:AB_10544537
Rabbit polyclonal anti-phospho-tau (S202)	Cell Signaling Technology	Cat# 11834
Rabbit polyclonal anti-phospho-tau (S262)	Thermo Fisher Scientific	Cat# 44-750G; RRID:AB_2533743
Mouse monoclonal anti-phospho-tau (S396/404)	Peter Davies	N/A
Rabbit polyclonal anti-KIBRA	Santa Cruz Biotechnology	Cat# sc-133374; RRID:AB_2216359
Rabbit polyclonal anti-PSD95	Cell Signaling Technology	Cat# 2507; RRID:AB_561221
Mouse monoclonal anti-AnkG	Santa Cruz Biotechnology	Cat# sc-12719; RRID:AB_626674
Rabbit polyclonal anti-βIV-spectrin	Matthew N. Rasband	N/A
Rabbit monoclonal anti-TNFα	Cell Signaling Technology	Cat# 11948; RRID:AB_2687962
Rabbit polyclonal anti-ac-p300/CBP	Cell Signaling Technology	Cat# 4771; RRID:AB_2262406
Rabbit polyclonal anti-DYKDDDDK tag	Cell Signaling Technology	Cat# 2368; RRID:AB_2217020
Rabbit polyclonal anti-cleaved caspase 3	Cell Signaling Technology	Cat# 9661 RRID:AB_2341188
Rabbit monoclonal anti-NeuN	Millipore	Cat# MABN140; RRID:AB_2571567
Mouse monoclonal anti-AnkG	UC Davis/NIH NeuroMab Facility	Cat# N106/36; RRID:AB_2877524
Alexa Flour 488 goat anti-mouse IgG (H+L)	Thermo Fisher Scientific	Cat# A-11001; RRID:AB_2534069
Alexa Flour 568 goat anti-rabbit IgG (H+L)	Thermo Fisher Scientific	Cat# A-11011; RRID:AB_143157
<b>Biological samples</b>		
Human plasma	The University of Texas Health Science Center at Houston	<a href="https://www.uth.edu">https://www.uth.edu</a>
Human cortical brain tissue	Mesulam Center for Cognitive Neurology and Alzheimer's Disease, Northwestern University	<a href="https://www.brain.northwestern.edu">https://www.brain.northwestern.edu</a>
<b>Chemicals, peptides, and recombinant proteins</b>		
CGP3466B maleate salt	Sigma-Aldrich	SML1941; CAS: 200189-97-5
Salsalate	AdipoGen	AG-CR1-3574; CAS: 552-94-3
P7C3-A20	Andrew A. Pieper	N/A
FK866 hydrochloride hydrate	Sigma-Aldrich	F8557; CAS: 658084-64-1 (free base)
EX527	Selleckchem	S1541; CAS: 49843-98-3
Diflunisal	Sigma-Aldrich	D3281; CAS: 22494-42-4

(Continued on next page)

***Continued***

REAGENT or RESOURCE	SOURCE	IDENTIFIER
<b>Critical commercial assays</b>		
Cytotoxicity Detection Kit (LDH)	Roche	Cat#04744926001
MACS Adult Brain Dissociation Kit	Miltenyi Biotec	Cat#130-107-677
MACS Neuronal isolation Kit	Miltenyi Biotec	Cat#130-115-389
Aurum Serum Protein Mini Kit	Bio-Rad	Cat#732-6701
NAD/NADH Quantitation Colorimetric Kit	Biovision	Cat#K337
FD NeuroSilver Kit	FD NeuroTechnologies, Inc	Cat#PK301
<b>Experimental models: cell lines</b>		
SH-SY5Y	ATCC	CRL-2266
<b>Experimental models: organisms/strains</b>		
Mouse: C57BL/6J (Stock No: 000664)	The Jackson Laboratory	RRID:IMSR_JAX:000664
Mouse: FVB.B-Wld <sup>S</sup> /UmonJ (Stock No: 008820)	The Jackson Laboratory	RRID:IMSR_JAX:008820
Mouse: Tg(Prnp-MAPT) #Lgn	Li Gan	RRID: MGI_5708386
Mouse: Tg(Prnp-MAPT*K274Q*K281Q)286Lgn	Li Gan	RRID: MGI_5708388
Rat: Long-Evans Rat	Envigo	Cat# 5508398; RRID: RGD_5508398
<b>Oligonucleotides</b>		
Primer CCL5 Forward: GGGTACCATGAAGATCTCTGC	This paper	N/A
Primer CCL5 Reverse: GCGAGGGAGAGGTAGGCAAAG	This paper	N/A
Primer IL-1 $\beta$ Forward: GAGCACCTTCTTTCTTCATCTT	This paper	N/A
Primer IL-1 $\beta$ Reverse: CACACACCAGCAGGTTATCATCA	This paper	N/A
Primer CCL2 Forward: GGCTCAGGCCAGATGCAGTTAA	This paper	N/A
Primer CCL2 Reverse: CCTACTCATTGGGATCATCTGCT	This paper	N/A
Primer GAPDH Forward: TGTGTCGTCGTGGATCTGA	This paper	N/A
Primer GAPDH Reverse: CCTGCTTCACCACCTTCTGA	This paper	N/A
<b>Recombinant DNA</b>		
Plasmid: Flag-TauWT	Li Gan	N/A
Plasmid: Flag-TauKQ	Li Gan	N/A
Plasmid: Flag-TauKR	Li Gan	N/A
<b>Software and algorithms</b>		
Any-maze	Stoelting	RRID: SCR_014289
ImageJ/Fiji	<a href="https://imagej.net/Fiji">https://imagej.net/Fiji</a>	RRID: SCR_002285
GraphPad Prism Version 9.0.0	<a href="https://www.graphpad.com/">https://www.graphpad.com/</a>	N/A
<b>Other</b>		
Zeiss LSM710 confocal microscope	Carl Zeiss	N/A
Zeiss Axiolmager.M2	Carl Zeiss	N/A
Zeiss Axio Scan.Z1	Carl Zeiss	N/A
CSU22 spinning disk confocal	Yokogawa Electric Corporation	N/A

**RESOURCE AVAILABILITY****Lead contact**

Further information and requests for resources and reagents should be directed to and will be fulfilled by the Lead Contact, Andrew A. Pieper ([Andrew.Pieper@HarringtonDiscovery.org](mailto:Andrew.Pieper@HarringtonDiscovery.org)).

**Materials availability**

This study did not generate new unique reagents.

**Data and code availability**

This study did not generate any new datasets or code.

## EXPERIMENTAL MODEL AND SUBJECT DETAILS

### Cell culture

SH-SY5Y cells were used to overexpress flag-tagged TauWT, TauKQ, TauKR for *in vitro* traumatic brain injury experiment. The cells were grown in DMEM:F12 (1:1)(GIBCO, 11320-033) containing 10% fetal bovine serum (GIBCO, 26140-079) and 1% penicillin/streptomycin (GIBCO, 15140-122).

### Animals

Male and female C57BL/6J (Stock No: 000664) mice were purchased from Jackson Laboratory. *Wld<sup>S</sup>* (Stock No: 008820) mice were purchased from Jackson Laboratory and bred at Louis Stokes Cleveland VA Medical Center under specific pathogen-free conditions. Twelve months old male and female TauWT and TauKQ<sup>high</sup> mice were used. Adult male Long-Evans outbred rats (Blue Spruce, HsdBlu:LE) were purchased from Envigo and approximately 3.5 months old rats were used. All animals were maintained under temperature, light, and humidity-controlled conditions with free access to food and water and randomly assigned to experimental groups. All animal work was approved by Louis Stokes Cleveland VA Medical Center Institutional Animal Care and Use Committee (animal protocol # 18-050-MS-18-015), University of California, San Francisco, Institutional Animal Care and Use Committee-approved guidelines, and Institutional Animal Care and Use Committees of the VA Western New York Healthcare System.

### Human subjects

Our experiments with human blood sample were approved by Institutional Review Board (IRB) (IRB Number HSC-MS-17-0776 (Molecular and Microbiome Mechanisms after Neurological Injury), HSC-MH-17-0452 (Biorepository of Neurological Disorders Registry and Tissue Repository at UT Health) and #EM-15-35 (University Hospitals Case Medical Center, Center for Clinical Research and Technology, OH). Written informed consent was obtained from the patient or surrogate. The average age of blood donors are  $54 \pm 11$  (controls) and  $48 \pm 20$  years old (TBI) and the majority are males (control 75%, TBI 88%). Sex and age information are reported in [Table S1](#).

Human brain samples were obtained from the holdings of Northwestern University Alzheimer's Disease Research Center brain bank, and under approved study protocols. All donors provided written informed consent for the use of brain tissue. The average age of tissue donors is  $81 \pm 5$  (group 1),  $83 \pm 7$  (group 2) and  $85 \pm 3$  years old (group 3). The history of TBI information is reported in [Results](#).

## METHOD DETAILS

### *In vitro* traumatic brain injury

SH-SY5Y cells were seeded at  $2 \times 10^6$  cells per well on the collagen I precoated 6-well flexible-bottomed culture plates (Flexcell International Corporation, BF-3001C). Flag-tagged TauWT, TauKQ and TauKR (provided by Dr. Li Gan) plasmids were transfected with FuGene® HD transfection reagent (Promega, E2311) according to the manufacturer's instructions. Six hours after transfection, cells were injured by 90-ms burst of pressurized medicinal air using the Cell Injury Controller II system (Custom Design & Fabrication Inc., Sandston, VA). Cells and culture media were harvested two hours after injury. LDH release was measured using a commercial assay kit (Cytotoxicity Detection Kit<sup>Plus</sup> (LDH), Roche, 04-744-926-001) according to the manufacturer's instructions.

### *In vivo* multimodal traumatic brain injury

Eight-week old male, female C57BL/6J and male *Wld<sup>S</sup>* mice were anesthetized with ketamine (100 mg/kg) and xylazine (10 mg/kg) via intraperitoneal (IP) injection and placed in an enclosed chamber constructed from an air tank partitioned into two sides and separated by a port covered by a mylar membrane. The pressure in the side not containing the mouse was increased to cause membrane rupture at 20 pounds per square inch (PSI), which generates a  $\sim$ 1-2 ms jet airflow of  $137.9 \pm 13.79$  kPa that passes through the animal's head. The head remains untethered in a padded holder, while the body is fully shielded by a metal tube. The jet of air produced upon membrane rupture provides a concussive injury, which is followed by acceleration/deceleration of the head and then exposure to the ensuing blast wave within an enclosed space.

### *In vivo* controlled cortical impact traumatic brain injury

Adult mice, 2 to 4 months of age, were anesthetized with ketamine (100 mg/kg) and xylazine (10 mg/kg) via intraperitoneal (IP) injection and placed on a heating pad to maintain body temperature. The animal's head was shaved and then placed on a stereotaxic frame where an incision was made through the skin, exposing the skull. For CCI injured mice, a  $\sim$ 5 mm diameter craniectomy was made over the right parietal cortex (bregma:  $-2.0$  mm; lateral  $-2.5$  mm), leaving the dura intact. Mice were then subjected to a moderate CCI injury with a piston velocity of 4.0 m/s and depth of 0.55 mm using an eCCI-6.0 device (Custom Design & Fabrication, Virginia Commonwealth, VA, United States). Sham controls underwent an identical surgical procedure with the absence of the craniectomy and injury. The incision was closed using 4-0 nylon non-absorbable sutures (Ethicon, Inc., Piscataway, NJ, United States), and mice were placed in a clean, single housed cage on a heating pad. For hydration and analgesia, animals were administered 1 mL of lactated ringer and 1.0 mg/mL buprenorphine. Ipsilateral CCI injured and sham cortices were harvested at 6 hr as well as 1, 3, 7, 21,

and 42 days post-injury. At the desired time points, mice were anesthetized with a ketamine/xylazine cocktail and euthanized by cervical dislocation, followed by dissection and freezing of injured and sham cortices.

### In vivo acoustic blast overpressure traumatic brain injury

We employed the shock tube device as described (Newman et al., 2015; Allen et al., 2018). The exit port of the shock tube is sealed by a thin brass foil diaphragm. With the diaphragm in place, the chamber behind the diaphragm is charged with compressed air, to a back pressure of 80 psi. A pressure sensor and air pressure modulator controlled by commercial hardware and custom software are used to charge the cylinder to the desired pressure. A computer-controlled (MATLAB) solenoid-driven hunting arrow mounted inside the chamber is used to pierce the diaphragm, once the criterion pressure is achieved; this triggers a blast with precise timing and sound pressure, which can be monitored by a pressure transducer probe placed at the outlet end of the shock tube and recorded by a commercial analog-to-digital converter and stored on a computer for later analysis using custom software. A wire mesh insert near the outlet end catches metal foil fragments (shrapnel), preventing penetrating injury to animals. Rats (adult male Long-Evans rats) were deeply anesthetized and placed into a custom-built metal holder, with body axis at right angles to the shock tube. Only the head was exposed (typically the left side), approximately 2.5 inches from the outlet end of the shock tube. A dual-blast paradigm, allowing a 1-month interval between blast exposures, each with a sound pressure of 63 kPa (190 dB-SPL) was employed. Animals were closely monitored at regular intervals for viability and any signs of distress following blast exposure.

### Metabolomics

Ten 8-week old male C57BL/6J mice were subjected to poly-traumatic brain injury as described above and ten were exposed to a sham-injury. Seven days post-injury, blood was collected retro-orbitally in K2-EDTA blood collection tubes. Plasma was separated from these blood samples and flash frozen in liquid nitrogen. Plasma samples were sent to Metabolon Inc, (Durham, North Carolina, USA) for Global Metabolomics Profiling using LC-MS. 245 biochemicals identified in these plasma samples were significantly different between TBI and Sham groups.

### Drug preparation and administration

CGP3466B (Sigma-Aldrich, SML1941) was dissolved in DMSO and then diluted in sterile saline. The final working stock was 0.0014 mg/ml for administering the 0.014 mg/kg dose. Intraperitoneal administration of CGP3466B was initiated 15 min or 24 h after injury, and tissues were harvested 6 h (for SNO-GAPDH, SNO-SIRT1 measurement) or 2 weeks (for ac-tau measurement) later, respectively. Salsalate (AdipoGen, AG-CR1-3574) was dissolved in DMSO and then diluted in sterile PBS. The final working stocks were as follows: 2.5 mg/ml (25 mg/kg dose), 1 mg/ml (10 mg/kg dose), 0.5 mg/ml (5 mg/kg dose). Daily intraperitoneal administration of salsalate was initiated 24 hr after injury and continued throughout behavioral testing. P7C3-A20 and FK866 (Sigma-Aldrich, F8557) were first dissolved in 1 vol of DMSO, followed by addition of 4 vol of Kolliphor and vigorously vortexing. The solution was then diluted with 30 vol of filtered 5% dextrose (pH 7.0). EX527 (Selleckchem, S1541) was dissolved in 1% DMSO + 30% polyethylene glycol + 1% Tween 80. Daily intraperitoneal administration of P7C3-A20 was initiated 24 hr after poly-traumatic brain injury. EX527 (10 mg/kg) was administered once a day and FK866 was treated twice per day, with the first injection given at the same time as P7C3-A20 (20 mg/kg) and the second injection given 6 h later (LoCoco et al., 2017). Diflunisal was first dissolved in 1 vol of DMSO, followed by addition of 2 vol of Kolliphor and vigorously vortexing. The solution was then diluted with 7 vol of saline to the appropriate concentration for administration at 25, 50, or 100 mg/kg.

### Behavioral analysis

The Barnes maze apparatus consisted of a gray circular platform (91 cm in diameter and 90 cm in height), with 20 equally spaced holes 5 cm in diameter along the perimeter (Stoelting Co.). One of these holes contained a recessed escape chamber located under the platform. Four different and equally-spaced visual cues with different shapes and colors were hung on a black circular curtain surrounding the maze. The training session consisted of four trials per day for four consecutive days. In each trial, the mouse was gently released in the middle of the maze under the cylindrical chamber, and after 5 s elapsed the covering chamber was lifted to allow the mouse to explore the maze. If a mouse failed to find the escape chamber within 60 s, it was manually guided to the escape chamber and then allowed to stay in the chamber for 30 s. Both the platform and the escape chamber were cleaned thoroughly between individual trials. On day 5, 24 h after the last training day, the escape chamber was removed and mice were allowed to explore the maze for 60 s. Total and primary latency were measured during training days, and latency to first nose pokes in escape hole and time spent in target quadrant were measured for memory test on the probe trial day. Any-maze video tracking software (Stoelting Co.) was used to acquire measurements. Analysis was conducted blind to treatment group.

For foot slip test of motor function, mice were trained to cross an 80 cm-long beam over two days and then tested on day 18. Video of the mice was recorded and analyzed by observers blind to treatment group.

### Western blotting

Western blotting was performed as described previously (Min et al., 2010), with the 9AB antibody against acetylated-tau generated in the Gan laboratory. Briefly, cortical and hippocampal tissues were sonicated in RIPA buffer (Sigma-Aldrich, R0278) containing protease and phosphatase inhibitor cocktail (Thermo Scientific, #1861284), 1 mM phenylmethyl sulfonyl fluoride (Sigma Aldrich, P7626),

and histone deacetylase inhibitors such as 5 mM nicotinamide (Sigma-Aldrich, 72340) and 1 µM trichostatin A (Sigma-Aldrich, T8552). Lysates were centrifuged at 170,000 g at 4°C for 15 min and at 18,000 g at 4°C for 10 min, after which protein concentrations of supernatants were measured by bicinchoninic acid assay (Thermo Scientific, A53225). Proteins were heated in a Laemmli Sample Buffer (Bio-Rad Laboratories, Inc., #1610737) with beta-mercaptoethanol (Bio-Rad Laboratories, Inc., #1610710) for 5 min, and then resolved in 4%-20% Criterion TGX Stain-Free gels (Bio-Rad Laboratories, Inc., #5678095). Stain-free gels were exposed to ultraviolet light by ChemiDocTM MP Imaging system (Bio-Rad Laboratories, Inc.) to visualize total plasma proteins. Proteins were transferred onto 0.2 µm polyvinylidene fluoride membranes (Bio-Rad Laboratories, Inc., #1704157) with the Trans-Blot Turbo system (Bio-Rad Laboratories, Inc.). Membranes were blocked with 5% nonfat dry milk in tris-buffered saline-tween 20 (TBST) for 1 h at room temperature, and then incubated with primary antibodies at 4°C overnight. The following antibodies were used to probe target proteins: rabbit anti-ac-tau (Li Gan laboratory, 1:500), mouse anti-tau (abcam, ab80579, 1:5000), mouse anti-tau (Thermo Fisher Scientific, #13-6400, 1:5000), mouse anti-β-actin (Santa Cruz Biotechnology, sc-47778, 1:1000), mouse anti-GAPDH (EMD Millipore Corp, MAB 374, 1:5000), mouse anti-NeuN (EMD Millipore Corp, MAB 377, 1:1000), mouse anti-GFAP (Thermo Scientific, MA5-12023, 1:1000), mouse anti-SIRT1 (Abcam, ab110304, 1:500), rabbit anti-p300 (Santa Cruz Biotechnology, sc-584, 1:500), rabbit anti-CBP (Cell Signaling Technology, #7389, 1:1000), rabbit anti-acetyl K5 histone 2A (Abcam, ab1764, 1:1000), rabbit anti-histone 2A (Cell Signaling Technology, #12349, 1:1000), rabbit anti-acetyl K18 histone 3 (Abcam, ab1191, 1:10,000), rabbit anti-histone 3 (Cell Signaling Technology, #4499, 1:1000), rabbit anti-phospho-tau (Ser 202) (Cell Signaling Technology, #11834, 1:1000), rabbit anti-phospho-tau (Ser 262) (Thermo Fisher Scientific, 44-750G, 1:1000), mouse anti-phospho-tau (Ser 396, 404) (gift from Dr. Peter Davies, 1:1000), rabbit anti-KIBRA (Santa Cruz Biotechnology, sc-133374, 1:500), rabbit anti-PSD95 (Cell Signaling Technology, #2507, 1:1000), mouse anti-AnkG (Santa Cruz Biotechnology, sc-12719, 1:1000), rabbit anti-βIV spectrin (gift from Dr. Matthew N. Rasband, 1:500), rabbit anti-TNF-alpha (Cell Signaling Technology, #11948, 1:2000), rabbit anti-ac-p300/CBP (Cell Signaling Technology, #4771, 1:1000), rabbit anti-Flag (Cell Signaling Technology, #2368, 1:1000), rabbit anti-cleaved caspase 3 (Cell Signaling Technology, #9661, 1:500). After primary antibody incubation, membranes were rinsed with TBST (3 × 5 min) and subsequently incubated with horseradish peroxidase conjugated-secondary antibodies. SuperSignalTM West Femto Maximum Sensitivity Substrate (Thermo Scientific, #34096) was used to detect band by BioSpectrum 810 Imaging System (UVP, Upland, CA). Densitometry quantification of western blot signal was conducted by ImageJ version 1.42 software (National Institutes of Health, Bethesda, MD).

### Neuron and non-neuron isolation

Three cortices were pooled and collected in DPBS with Calcium, Magnesium, Glucose and Pyruvate (Thermo Fisher Scientific, 14287080) and processed using the MACS Adult Brain dissociation kit (Miltenyi Biotec, 130-107-677) to generate a single cell suspension. Briefly, each sample was digested using a combination of enzymatic and mechanical dissociation. For enzymatic dissociation, Enzyme mixes 1 and 2 (provided in the kit) were used for mechanical dissociation. Samples immersed in the enzymes mixes were placed in MACS C-tubes, which were placed in the MACS Octo dissociator with heaters for 30 min at 37°C. The dissociated samples were further processed for debris removal by first passing them through a MACS 70 µm smart strainer and then using MACS Debris Removal reagent. Lastly, RBC lysis was performed to achieve the final single cell suspension of brain cells. This single cell suspension was further processed using the MACS Neuronal isolation kit (Miltenyi Biotec, 130-115-389) to separate the single cell suspension into neuronal and non-neuronal populations. Briefly, cells were mixed with MACS Non-neuronal cell Biotin antibody cocktail for 5 min. After washing with DPBS (with 0.5% FBS), cells were incubated with Anti-Biotin Microbeads. After a 10-min incubation, cells were passed through a column attached to a magnetic stand, which results in binding of non-neuronal cells (labeled by microbead-biotin antibodies) to the column, and the flow-through was collected as neuronal population. The non-neuronal population was collected by removing the column from the magnetic stand and placing the plunger in the column to flush out the non-neuronal cells.

### SNO-resin assisted capture (SNO-RAC)

SNO-RAC was performed as described previously (Forrester et al., 2009). Mouse cerebral cortex was mechanically homogenized in lysis buffer containing 100 mM HEPES/1 mM EDTA/0.1 mM neocuproine (HEN), 150 mM NaCl, 0.1% (vol/vol) Nonidet P-40 (NP-40), 0.2% S-methylmethanethiosulfonate (MMTS) and protease and phosphatase inhibitor cocktail (Thermo Scientific, #1861284). After two times centrifugation (20,000 g at 4°C for 20 min), protein concentration of supernatants was determined using Coomassie protein assay (Thermo Scientific, #1856210). Total lysates were treated with 0.2% MMTS and 2.5% SDS, and then incubated at 50°C for 20 min. Proteins were precipitated with pre-chilled (-20°C) acetone and centrifuged at 4,255 g at 4°C for 12 min. After washing pellets with 70% acetone three times, proteins were sonicated in HEN buffer containing 1% SDS. Precipitation of proteins was repeated with -20°C acetone, and the final pellets were resuspended in HEN/1% SDS. Proteins were incubated with freshly prepared 30 mM ascorbate and 50 µl of thiopropyl Sepharose (GE Lifesciences, 17-0420-01, Pittsburgh, PA) and rotated in the dark for 3 h. After centrifugation at 1,200 g for 30 s, the bound SNO proteins were sequentially washed three times with HEN/1%SDS and two times with 1/10 diluted HEN/1%SDS. SNO-proteins were then eluted with 2 x Laemmli Sample Buffer (Bio-Rad Laboratories, Inc., #1610737) with 10% beta-mercaptoethanol (Bio-Rad Laboratories, Inc., #1610710) and analyzed by SDS-PAGE and immunoblotting.

### Postsynaptic density fractionation

To enrich the postsynaptic density (PSD), synaptosomal membranes were isolated from adult mice following Kristian et al., 2010 with minor modifications (Kristian, 2010; Cao et al., 2007). Brains were extracted, and the cortex and hippocampus were quickly dissected. Tissue samples were immediately homogenized with 8 passes of a Teflon on glass Potter-Elvehjem homogenizer in sub-cellular isolation buffer (SIB: 225 mM mannitol, 75 mM sucrose, 2 mM K2HPO<sub>4</sub>, 5 mM HEPES, 1 mM EGTA, 0.1% fatty acid free bovine serum albumin). Differential centrifugation was performed at 1,500 g followed by 21,000 g on the supernatant to sequentially de-enrich unlysed cells and cytosolic and endoplasmic reticulum proteins, respectively. The resulting membrane-enriched pellet was separated at 21,000 g for 8 minutes over a discontinuous Percoll gradient comprised of 15%, 24%, and 40% Percoll steps. Synaptosomes were collected between the 15% and 24% Percoll interfaces. Synaptosomes diluted in SIB were pelleted at 10,000 g. All steps were performed on ice with centrifuging at 4°C.

### Immunohistochemistry

Mice were transcardially perfused with cold 1 x phosphate-buffered saline (PBS) followed by 4% paraformaldehyde in PBS at pH 7.4 under anesthesia. Brains were carefully removed and post-fixed in 4% paraformaldehyde for 24–48 h at 4°C. Brains were immersed in 30% sucrose in PBS for 48–72 h at 4°C and then rapidly frozen in 2-methylbutane pre-cooled to –20°C with dry ice. Brains were cut coronally (30 or 40 µm) and sections were stored in cryoprotective solution (150 mM Ethylene glycol, 100 mM glycerol, 250 mM PBS) at -20°C. For tau and NeuN staining, sections were washed three times with PBS for 5 min and then treated with 0.2% Triton X-100 in PBS for 15 min. Sections were washed with PBS and then incubated with 100 mM glycine for 15 min. After blocking sections using blocking buffer (1% bovine serum albumin, 10% normal goat serum, 0.3 M glycine) for 30 min, primary antibodies (Tau, Thermo Fisher Scientific, #13-6400, 1:100, NeuN, EMD Millipore Cor., #MABN-140, 1:500) were incubated overnight at 4°C. Sections were washed three times with PBS (5 min each) and then incubated with Alexa Fluor 488 goat anti-mouse (Thermo Fisher Scientific, A11001, 1:200) or Alexa Fluor 568 goat anti-rabbit (Thermo Fisher Scientific, A11011, 1:200) at room temperature for 2 h. Sections were mounted on slides and then coverslipped with Prolong diamond antifade mountant (Invitrogen, P36961). AnkG and βIV spectrin staining were performed as described previously (Sohn et al., 2016). Sections were permeabilized with 0.3% Triton X-100 and blocked with 10% normal goat serum at room temperature for 1 h. Sections were incubated with primary antibodies (AnkG, UC Davis/NIH NeuroMab Facility, N106/36, 1:500, βIV spectrin, gift from Dr. Matthew N. Rasband, 1:500) overnight at 4°C and then with Alexa Fluor 488 goat anti-mouse (Thermo Fisher Scientific, A11001, 1:300) or Alexa Fluor 568 goat anti-rabbit (Thermo Fisher Scientific, A11011, 1:300) at room temperature for 1 h. For synaptic vesicle 2 staining, brain sections were first permeabilized in blocking solution containing PBS with 0.5% Triton X-100 and 10% normal donkey serum for 1 h at room temperature. Then they were incubated overnight with an SV2 antibody (Developmental Studies Hybridoma Bank) in blocking solution followed the next day by a 1 h incubation with an Alexa-conjugated secondary antibody (Life Technologies) at room temperature. For silver staining, sections were collected in 0.1 M phosphate buffer (pH 7.4) containing 4% paraformaldehyde and fixed for 7 days at 4°C. Sections were then processed for the detection of axon degeneration with FD NeuroSilver Kit II (FD Neurotechnologies, PK301) according to the manufacturer's instructions. Sections were subsequently mounted on slides, cleared in xylene, and coverslipped with Permount (Fisher Scientific, Fair Lawn, NJ).

### Quantification of immunohistochemistry

Images were acquired with Zeiss LSM710 confocal microscope, Zeiss AxioImager.M2 with monochromatic digital camera (Zeiss AxioCam MRm Rev. 3) and Zeiss Axio Scan.Z1. To visualize the axon initial segment, twenty serial optical sections (0.5 µm steps) were projected into a single image. Confocal images of synaptic vesicle 2 were acquired on a CSU22 spinning disk confocal system (Yokogawa) with a Ti-E microscope (Nikon) using a 60x oil immersion objective lens. ImageJ version 1.42 software (National Institutes of Health, Bethesda, MD) was used to analyze the intensity of the AIS, tau, SV2 and integrated density of silver staining with the plugin of the color deconvolution method as previously described (Ruifrok and Johnston, 2001). The operator performing quantification was blinded to condition and treatment.

### Quantitative real-time PCR

Total RNA was extracted from frozen cortex using High Pure RNA Isolation Kit (Roche Life Science, USA) according to the manufacturer's protocol. RNA concentrations were determined by UV visible absorption spectra, using Nanodrop 2000 (Thermo Scientific, USA). First-strand cDNA was synthesized from total RNA (500ng) using iScript cDNA Synthesis Kit (Bio-Rad Laboratories Inc., 1708891, USA) according to the manufacturer's instruction. Quantitative PCR was performed in triplicate using Fast SYBR Green Master Mix on a Step One Plus Real-time PCR System (Applied Biosystems, USA). Following primers (5' to 3') were used to examine the gene expression of CCL5, IL1β, CCL2, and GAPDH; CCL5 (F): GGG TAC CAT GAA GAT CTC TGC, (R): GCG AGG GAG AGG TAG GCA AAG, IL-1β (F): GAG CAC CTT CTT TTC CTT CAT CTT, (R): CAC ACA CCA GCA GGT TAT CAT CA, CCL2 (F): GGC TCA GCC AGA TGC AGT TAA, (R): CCT ACT CAT TGG GAT CAT CTT GCT, GAPDH (F): TGT GTC CGT CGT GGA TCT GA, (R): CCT GCT TCA CCA CCT TCT TGA. Fold change of gene expression was calculated by comparative CT quantification method (Schmittgen and Li-vak, 2008) and normalized to the expression of GAPDH.

**NAD<sup>+</sup> measurement**

Cerebral cortex was dissected as quickly as possible on a cold metal block and flash frozen in liquid nitrogen. Samples were stored at -80°C until assay. Tissue NAD<sup>+</sup> determination was performed according to the manufacturer's instructions (BioVision, K337-100). Brain tissues were washed with cold PBS and homogenized in NADH/NAD extraction buffer and then centrifuged at 14,000 rpm at 4°C for 15 min. Supernatants were filtered using 3 kDa molecular weight cutoff centrifugal filters (Merck Millipore Ltd., UFC500324) to remove enzymes that consume NADH and NAD. Fifty microliters of samples were transferred into a 96 well plate for total NADH and NAD, and 50 µl of sample was heated at 60°C for 30 min to decompose NAD and then also added into a 96 well plate for measuring total NADH. Ten microliters of 1 nmol/µl NADH standard was diluted with 990 µl of NADH/NAD extraction buffer and then transferred into a 96 well plate to make 0, 20, 40, 60, 80, and 100 pmol/well. One hundred microliters of NAD cycling enzyme mix was added into standard, and samples were then incubated in the plate at room temperature for 5 min. After adding 10 µl of NADH developer, the plate was read at OD 450 nm.

**Preparation of plasma and albumin/immunoglobulin depletion**

Mice were anesthetized with ketamine (100 mg/kg) and xylazine (10 mg/kg) via intraperitoneal (IP) injection and blood samples were collected in EDTA tubes (Becton, Dickinson and Company, 365974) by retro-orbital bleeding and then plasma was separated at 2,000 g at 4°C for 15 min. Albumin and immunoglobulin depletion were performed according to the manufacturer's instructions (Bio-Rad Laboratories, Inc., 732-6701). Briefly, Aurum serum protein columns were washed two times with 1 mL of Aurum serum protein binding buffer and centrifuged at 10,000 g for 20 s. Sixty microliter of human and mouse plasma sample was mixed with 180 µl of Aurum serum protein binding buffer and 200 µl of the diluted plasma sample were added to the top of the resin bed. Column was gently vortexed every 5 min for a total incubation time of 15 min and then centrifuged at 10,000 g for 20 s. Eluate was collected in collection tube and resin was washed with 200 µl of the binding buffer. After centrifugation (10,000 g, 20 s), the eluate was collected in a previous collection tube.

**Tau seed amplification assay (AD RT-QuIC)**

Twenty percentage w/v brain homogenates were prepared from hippocampus and cortex in ice-cold 1X PBS with protease inhibitors (Roche, complete, EDTA-free) using 1 mm zirconia/silica beads (Biospec Products) and a BeadMill 24 (Fisher Scientific). Brain homogenates were used to seed the AD RT-QuIC. Assay conditions used were as previously published ([Kraus et al., 2019](#)) with the addition that both heparin (USP, 1235820) and poly-L-glutamate (Sigma, P1818) were independently tested in evaluating seeding activity. Synthetic fibrils generated from recombinant tau encoding aa 306-378 were used as a positive control. For analysis of human TBI and control plasma samples (albumin/immunoglobulin depleted), 5 µl was used to seed the reaction, with triplicate wells analyzed for each biological replicate. 18 ng of synthetic fibrils / 5 µl of control plasma was used as a positive control to verify that plasma matrices were not inhibitory to the RT-QuIC reactions.

**Quanterix**

Plasma NfL, UCH-L1, GFAP, pTau181 and Tau from control and TBI patient's samples were measured by using Simoa® Neurology 4-Plex B kit and Simoa® pTau-181 advantage V2 kit by Quanterix The Science of Precision Health (Billerica, MA).

**Diflunisal pharmacokinetics**

Diflunisal levels in mouse plasma and brain were monitored by LC-MS/MS using an AB Sciex (Framingham, MA) 4000 QTRAP® mass spectrometer coupled to a Shimadzu (Columbia, MD) Prominence LC. Diflunisal was detected with the mass spectrometer in negative MRM (multiple reaction monitoring) mode by following the precursor to fragment ion transitions 248.9 to 204.9 (quantifier ion) and 248.9 to 184.9 (qualifier ion). An Agilent C18 XDB column (5 micron, 50 X 4.6 mm) was used for chromatography for PK studies with the following conditions: Buffer A: dH2O + 0.1% formic acid, Buffer B: acetonitrile + 0.1% formic acid, 0 - 1.0 min 5% B, 1.0 - 1.5 min gradient to 100% B, 1.5 - 3.0 min 100% B, 3.0 - 3.2 min gradient to 5% B, 3.2 - 4.5 5% B. Tolbutamide (transition 269.1 to 169.9) from Sigma (St. Louis, MO) was used as an internal standard (IS). Pharmacokinetic studies were performed by injecting 8 week old C57BL/6J male mice with diflunisal formulated in 10% DMSO, 20% Kolliphor EL, 70% saline. 60 or 180 minutes post-dose, animals were anesthetized with ketamine (100 mg/kg) and xylazine (10 mg/kg) via intraperitoneal (IP) injection. Blood was collected using the anti-coagulant ACD, and then brains were harvested after transcardial perfusion with 1xPBS. Tissues were weighed before snap freezing and blood spun at 2,000x g at 4°C for 15 min to collect plasma which was stored frozen along with brain tissue at -80°C until analysis. Brain tissue was homogenized in a 3-fold volume (weight by volume) of PBS to generate a homogenate. 100 µl of plasma or tissue homogenate was mixed with 100 µl of acetonitrile plus 0.2% formic acid and 100 ng/ml N-benzylbenzamide IS. The samples were vortexed 15 s, incubated at room temp for 10' and spun twice at 16,100 x g 4°C in a refrigerated microcentrifuge. Standard curves were generated using blank plasma (Bioreclamation, Westbury, NY) or blank tissue homogenate spiked with known concentrations of diflunisal and processed as described above. The concentration of drug in each time-point sample was quantified using Analyst software (Sciex). A value of 3-fold above the signal obtained from blank plasma or tissue homogenate was designated the limit of detection (LOD). The limit of quantitation (LOQ) was defined as the lowest concentration at which back calculation yielded a concentration within 20% of theoretical.

### Diflunisal protein binding

Protein binding of diflunisal in mouse plasma or brain homogenate was determined by rapid equilibrium dialysis using RED chambers (Thermo Scientific, Waltham, MA). On the day of the RED experiment, frozen mouse plasma and 4x homogenized brain was thawed in a water bath at 37°C. Then it was equilibrated for 45 minutes at 37°C in an atmosphere of 5% CO<sub>2</sub>. The pH of PBS was confirmed within 7.4 ± 0.1. The pH of plasma and brain was measured and adjusted to 7.4 ± 0.1 using concentrated acid or base. Plasma and brain were diluted at 1:20 (final) with PBS and used for all subsequent steps. An aliquot of plasma or brain was spiked with compound to a compound concentration of 5 µM and vortex mixed. Enough non-spiked matrix remained to enable matrix matching of dialysate at the end of the binding assessment. This matrix was stored at 37°C in an atmosphere of 5% CO<sub>2</sub>. For each matrix, dialysis was performed using n = 4 individual RED units with 200 µL of compound spiked plasma or brain homogenate at 5 µM in the donor chamber and 400 µL of PBS in the dialysate chamber. The plate containing the RED units was sealed with a gas-permeable seal and incubated at 37°C for 6 hours under a 5% CO<sub>2</sub> atmosphere in an orbital shaker set to 100 rpm. At the end of the dialysis period, aliquots were taken from the donor and dialysate chambers of each RED unit to obtain post-dialysis measures of bound and unbound compound concentration. Donor, dialysate, and plasma or brain stability samples were analyzed by using a matrix matching approach whereby each sample was mixed in a 1:1 ratio with the opposite medium (blank matrix or PBS). The matrix matched samples were then crashed with 200 µL acetonitrile + formic acid (0.1% final) + tolbutamide IS (50 ng/mL final). Tubes were vortex mixed for 10 s and incubated at room temperature for 10 minutes. Then they were centrifuged at 16,100 x g for 5 minutes. Diflunisal levels in both chambers were measured by LC-MS/MS in comparison to a standard curve prepared in 1:1 matrix:PBS as described above. For each matrix, stability was assessed by maintaining individual aliquots of compound-spiked matrix at 37°C and 5% CO<sub>2</sub> for 0 and 6 hours. At each time point, n = 2 50 µL aliquots were matrix matched and crashed. Stability of diflunisal in plasma and brain was 99% over 6 hours as assessed by LC-MS/MS. Fraction unbound (f<sub>u</sub>) was determined based on the following equations:

$$f_u = \frac{C_{\text{dialysate}}}{C_{\text{donor}}}$$

$$\text{DF} = \frac{\text{Total volume of solution}}{\text{volume of aliquot}}$$

$$f_{u \text{ undiluted}} = \frac{1/\text{DF}}{((1/f_u \text{ diluted}) - 1) + 1/\text{DF}}$$

f<sub>u</sub> – fraction unbound

C<sub>dialysate</sub> – concentration of compound in dialysate chamber after dialysis

C<sub>donor</sub> – concentration of compound in donor chamber after dialysis

DF – dilution factor for plasma dilution

f<sub>u undiluted</sub> – fraction unbound after correcting for plasma dilution

f<sub>u diluted</sub> – fraction unbound of diluted plasma, calculated using the f<sub>u</sub> equation above if using diluted plasma

### Human plasma study

This is a retrospective study of plasma samples from subjects with TBI admitted to the neuroscience intensive care unit at the Memorial Herman Hospital-Texas Medical Center from December 2017 to April 2019. Inclusion criteria were age > 18, presented after TBI (ACRM criteria: loss of consciousness, posttraumatic amnesia, alteration of consciousness), underwent a brain CT, fluency in English or Spanish, ability to provide consent (or consent obtainable from surrogate), visual acuity/hearing adequate for testing and neurologically intact prior to injury. Exclusion criteria were patients with past medical history (including bipolar disorder, seizures, dementia, depression, schizophrenia, HIV, cancer (current treatment that would interfere with follow-up), end-stage renal disease (on dialysis), severe polytrauma that would interfere with follow-up, modified Rankin scale (mRS) > 1 (i.e., uses walker or need assistance with daily actives), claustrophobia, lives greater than 2 hour from hospital, low interest/low probability for follow-up, prisoner, pregnant women, penetrating TBI, current participation in interventional trial and risk of imminent death. Blood samples were collected at 5 pre-determined time-points: < 24 hours of injury (T1), during 24–48 hours of injury (T3), during 3–5 days of injury (T4), during 6–8 days of injury (T5) and > 10 days after injury (T6). We randomly selected 45 subjects, age- and gender-matched with 25 non-neurologically-impaired healthy subjects. Eighty-nine TBI plasma samples were analyzed: 44 at T1, 22 at T3, 6 at T4, 7 at T5, and 10 at T6. Since fewer samples were collected after T1, results obtained from T3 and T4 (24–120 hours post-TBI), and from T5 and T6 (> 120 hours post-TBI), were grouped for analysis. Mean participant age (±SD) was 50 ± 18 years, and average age between TBI patients and healthy subjects was similar (48 ± 20 versus 54 ± 11, p > 0.05; Table S1). Sex-ratio was equivalent across TBI and controls (89% versus 75% male, p > 0.05). Due to myriad reasons, samples from all patients at all time-points are not available. Blood was drawn from existing lines or by venipuncture and collected into sterile vacutainers per time point. The samples were placed on ice

immediately after collection and transported to the laboratory for centrifugation within an hour of draw (at 1460 x g for 10 minutes at 4°C), generating plasma. The plasma was centrifuged a second time (at 1460 x g for 10 minutes at 4°C) in order to generate platelet-poor plasma. Plasma was divided into aliquots and frozen at -80°C until analysis. Based on admission GCS, subjects were grouped by injury grade as mild (GCS between 13 and 15), moderate (GCS between 9 and 12) and severe (GCS less than 9). During the study period, 85 TBI subjects were consented (27 mild, 23 moderate, 34 severe and 1 unknown). From these subjects, we randomly selected 45 subjects: 15 mild TBI subjects, 15 moderate TBI subjects and 15 from severe TBI so that subjects across injury severity grade (mild, moderate or severe) were matched for age. Additionally, all TBI subjects (n = 45) were also matched for age and sex with respect to the control subjects. Plasma samples from 25 non-neurological subjects were used as controls (patients were approached and enrolled at the UT Physician Cardiology clinic). Blood was drawn by venipuncture and collected into sterile vacutainers and immediately placed on ice. For processing of plasma, the tubes were centrifuged at 1460 x g for 10 minutes at 4°C followed by a second centrifugation at 1460 x g for 10 minutes at 4°C to generate platelet-poor plasma. Plasma was then aliquoted and stored at -80°C until analysis. Demographic and clinical information including past medical history, age, sex, Glasgow coma scale (GCS) at admission. Descriptive statistics were calculated for demographic variables in TBI and control cohorts (Table S1). To describe differences in age and sex, we used the Student's t test,  $\chi^2$ -test, and Fisher's exact test. Statistical analyses were performed using open-source software packages in R (v3.1.3).

### Human brain study

Nine human brain specimens were obtained from the holdings of Northwestern University Alzheimer's Disease Research Center brain bank, as described in the Results section, with results displayed in Figure 6J.

### Pharmacoepidemiologic validation

The IBM® MarketScan® Medicare Supplemental Database is one of the first in the U.S. to profile the healthcare experience of retirees with Medicare supplemental insurance paid by employers. The MarketScan® Medicare Supplemental Database provides detailed cost, use and outcomes data for healthcare services performed in both inpatient and outpatient settings. For most of the population, the medical claims are linked to outpatient prescription drug claims and person-level enrollment data through the use of unique patient or enrollee identifiers. Beneficiaries in the MarketScan® Medicare Supplemental Database have drug coverage; therefore, drug data are available and provide additional, often valuable, information. This feature makes the database a robust tool for pharmacoeconomic and outcomes research and helps provide insight into the drug use and spending patterns of older Americans. In this study, the pharmacoepidemiology study utilized the MarketScan® Medicare Claims database from 2012 to 2017. The dataset included individual-level diagnosis codes, procedure codes and pharmacy claim data for 7.23 million patients. Pharmacy prescriptions of salsalate, diflunisal, and aspirin were identified by using RxNorm and National Drug Code (NDC). For a subject, a drug episode is defined as from drug initiation to drug discontinuation. Specifically, drug initiation is defined as the first day of drug supply (i.e., 1st prescription date). Drug discontinuation is defined as the last day of drug supply (i.e., last prescription date + days of supply) and without drug supply for the next 60 days. In another word, gaps of less than 60-day of drug supply were allowed within a drug episode. The drug cohort included the first drug episode for each subject. For the final cohorts, demographic variables including age, race, sex and geographical location were collected. Additionally, diagnoses of hypertension (HT), type 2 diabetes (T2D), and coronary artery disease (CAD) before drug initiation were collected (Table S3). These variables were specifically selected to address potential confounding biases. Last, a control cohort was selected from patients who were not exposed to salsalate and diflunisal. Specifically, control exposures were matched to the exposures (n strata = 10) by initiation time, enrollment history, gender, HT diagnose, T2D diagnose and CAD diagnose. The outcome was time from drug initiation to diagnose of AD and TBI defined by ICD9/10 codes (Table S4). For drug cohorts, observations without diagnosis of AD were censored at the end of drug episodes. For the control cohort, the corresponding drug episode starting date was used as the starting time. Observations without diagnosis of AD were censored at the corresponding drug episode's end date. The detailed description are provided in a previous study (Cheng et al., 2018). For propensity score estimation, we define NE = north east, NC = north central, S = south, W = west, T2D = type 2 diabetes, HT = hypertension and CAD = coronary artery disease. The propensity score of taking a candidate drug versus a comparator drug (i.e., aspirin) was estimated by the following logistic regression model:

$$\text{logit}[\Pr(\text{candidate drug} = 1)] = \beta_0 + \beta_1 \text{Age} + \beta_2 \text{Gender} + \beta_3 \mathbf{1}(\text{Location} = \text{NE}) + \beta_4 \mathbf{1}(\text{Location} = \text{NC}) \\ + \beta_5 \mathbf{1}(\text{Location} = \text{S}) + \beta_6 \mathbf{1}(\text{Location} = \text{W}) + \beta_7 \text{T2D} + \beta_8 \text{HT} + \beta_9 \text{CAD}.$$

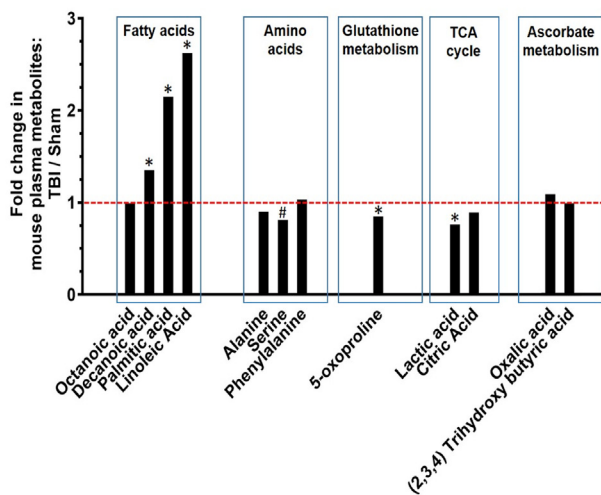
Stratified Cox models were used to compare the TBI or AD risks. For a candidate drug (i.e., salsalate or diflunisal) versus a comparator drug (i.e., aspirin), the analyses were stratified (n strata = 10) by the estimated propensity score. All analyses were stratified based on the subgroups defined by sex, T2D, HT and CAD diagnoses (n strata = 10). Finally, propensity score stratified Cox-proportional hazards models were used to conduct statistical inference for the hazard ratios (HR) of developing AD or TBI between cohorts.

**QUANTIFICATION AND STATISTICAL ANALYSIS**

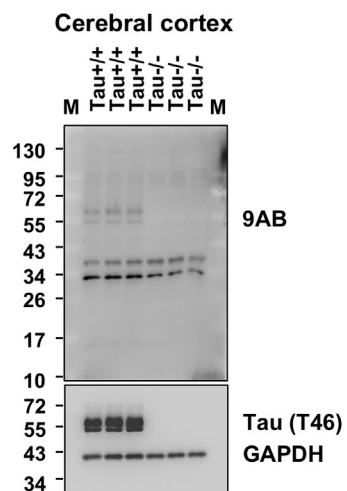
All statistical analyses were performed using GraphPad Prism, version 9.0.0 (GraphPad Software, Inc.). Student's t test was used to demonstrate statistical differences between two groups, and One-way ANOVA or repeated-measured two-way ANOVA with Dunnett's or Tukey's post hoc test was used when appropriate. Values are presented as mean  $\pm$  SEM, and individual data points represent individual samples or animals. Details of statistical analysis can be found in the figure legends (statistical tests used, what n represents, etc.). Significance was determined at p value below of 0.05, while p values below or equal to 0.05, 0.01, 0.001 and 0.0001 were represented by \*, \*\*, \*\*\* and \*\*\*\*, respectively.

# Supplemental figures

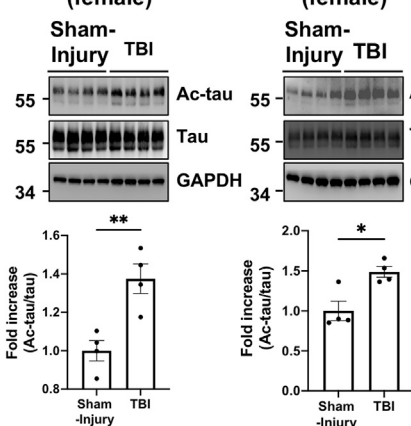
**A**



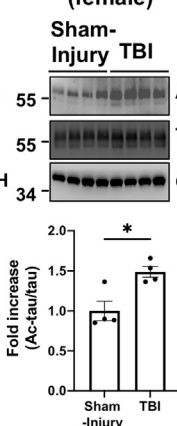
**B**



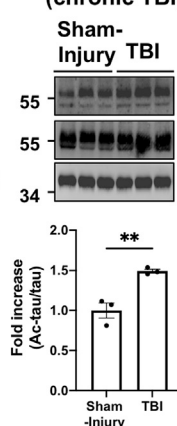
**C Cerebral cortex (female)**



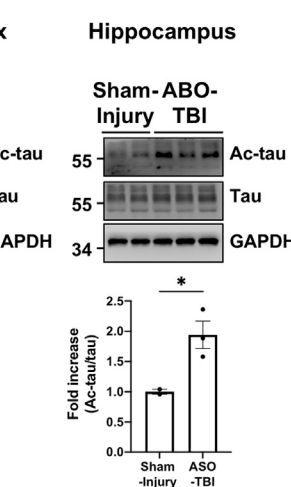
**Hippocampus (female)**



**D Cerebral cortex (chronic TBI)**

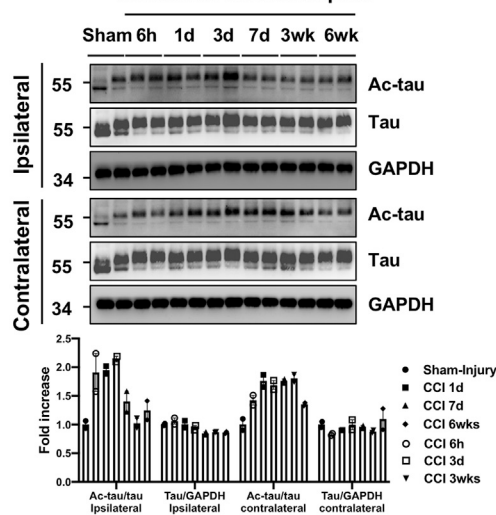


**E Cerebral cortex**

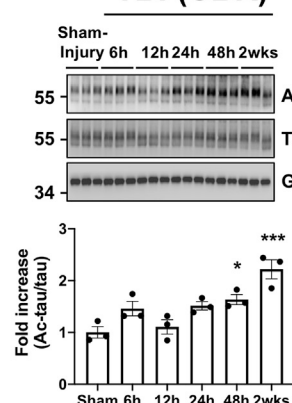


**Hippocampus**

**F Cerebral cortex**  
Controlled Cortical Impact

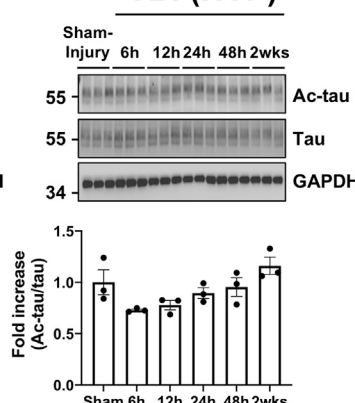


**G TBI (CBR)**



**TBI**

**H TBI (HYP)**

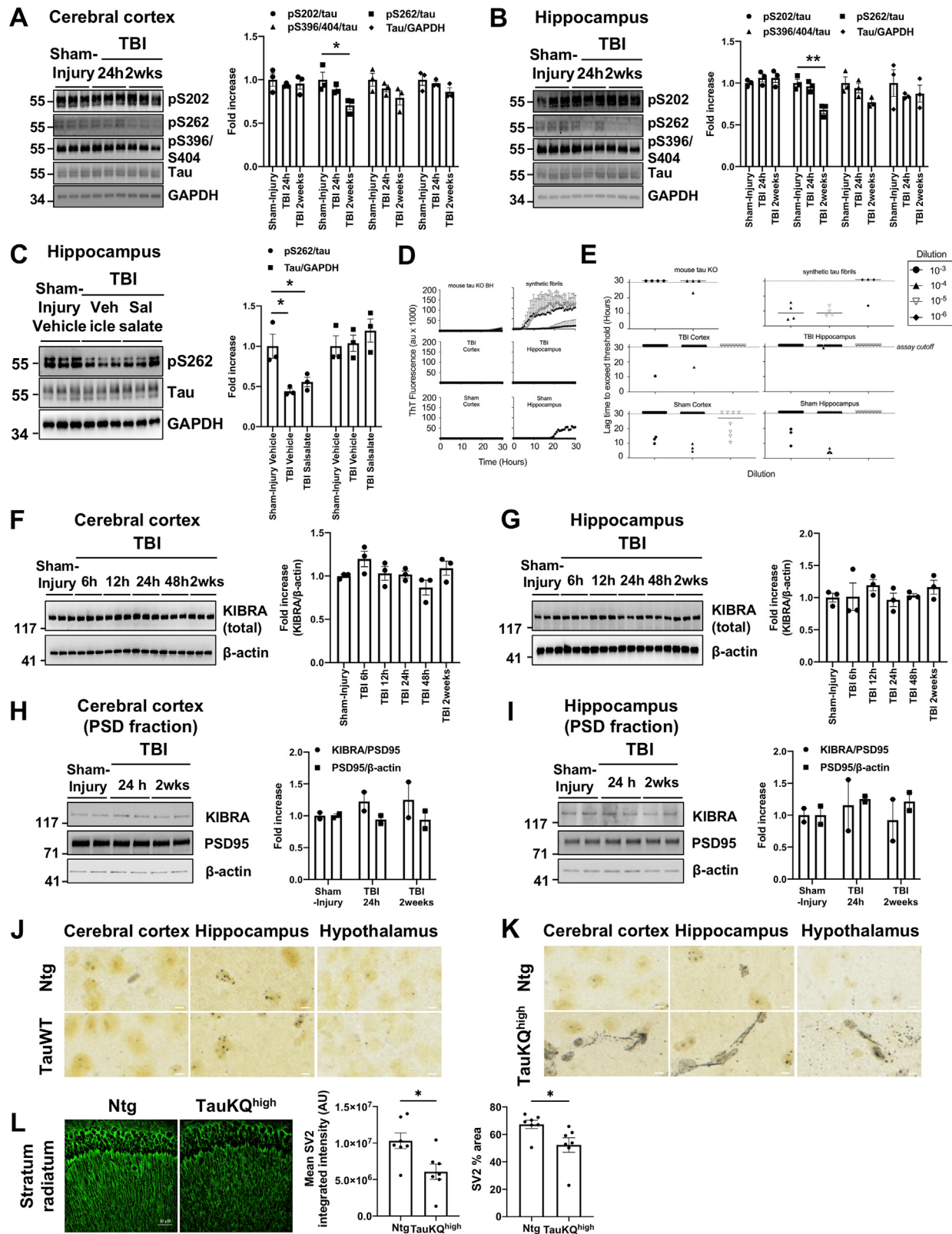


**TBI**

(legend on next page)

**Figure S1. Metabolite and ac-tau analysis after TBI, related to Figure 1**

- (A) Nonbiased whole-metabolome analysis of mouse plasma 1 week after TBI or sham injury of 8-week old C57BL/6J mice shows alterations in plasma levels of metabolites in fatty acid (decanoic acid, palmitic acid, linoleic acid), amino acid (serine), glutathione (5-oxoproline), and TCA cycle (lactic acid) pathways consistent with what has been previously reported in human TBI plasma. (n = 10 per group, \*p < 0.05, # trending).
- (B) 9AB antibody generated by the Gan laboratory against mouse tau acetylated at K263 and K270 recognizes ac-tau in brain extract from wild-type mice, but not from tau knockout mice. The presence or absence of tau in wild-type or tau knockout mice, respectively, was confirmed by western blot for tau with T46 antibody (Invitrogen). Western blot for GAPDH shows equal loading of protein across lanes. (M = molecular weight marker lanes)
- (C) western blot and its quantification show that a single TBI increases ac-tau in cerebral cortex and hippocampus of female mice 2 weeks later. (Each group n = 4, \*p < 0.05, \*\*p < 0.01 versus Sham-Injury group, Student's t test).
- (D) western blot and its quantification show that ac-tau is significantly increased 17 months after a single TBI in male C57BL/6J mice (Each group n = 3, \*\*p < 0.01 versus Sham-Injury group, Student's t test).
- (E) western blot and its quantification show that cortical and hippocampal ac-tau are significantly increased 7 months after acoustic blast overpressure-injury in male Long-Evans rats (Each group n = 2-3, \*p < 0.05 versus Sham-Injury group, Student's t test).
- (F) western blot and its quantification show that controlled cortical impact injury of male wild-type mice increased ac-tau in the ipsilateral (6h, 1d, 3d after injury) and contralateral side (1d, 3d, 7d, 3 wks), with no change in total tau levels (Each group n = 2).
- (G) western blot and its quantification show increased ac-tau 48 h – 2 weeks after TBI in cerebellum (Each group n = 3, \*p < 0.05, \*\*\*p < 0.001 versus Sham-Injury group, one-way ANOVA with Dunnett multiple comparisons test).
- (H) western blot and its quantification show no increase in hypothalamic ac-tau after TBI (Each group n = 3).



(legend on next page)

**Figure S2. Tau acetylation after TBI is not associated with increased tau phosphorylation, altered tau levels, altered tau seeding capacity, or kidney/brain (KIBRA) expression is unchanged after TBI, and TauKQ<sup>high</sup> animals display elevated axon degeneration and reduced synapses, related to Figure 1**

(A), (B) western blot and its quantification show no increase in tau phosphorylation at residues S202, S262, S396, and S404, either 24 hours or 2 weeks after TBI. Phosphorylation of tau at S262 is significantly decreased in cortex and hippocampus 2 weeks after TBI (Each group n = 3, \*p < 0.05, \*\*p < 0.01 versus Sham-Injury group, one-way ANOVA with Dunnett multiple comparisons test).

(C) western blot and its quantification show that phosphorylation of tau at S262 remains significantly decreased in hippocampus even when acetylation of tau is blocked by treating mice after TBI with the p300/CBP inhibitor salsalate (Each group n = 3, \*p < 0.05 versus Sham-Injury group, one-way ANOVA and Tukey's post hoc analysis).

In (A), (B), and (C), total tau levels remained constant at all times after TBI.

(D) TBI and sham-injury brain homogenates were used to seed the Alzheimer's disease real-time quaking-induced conversion (AD RT-QuIC) assay. Each curve represents the thioflavin T (ThT) fluorescence readouts of the mean ± SD of quadruplicate wells seeded at the dilutions indicated.

(E) Lag time to exceed the ThT fluorescence threshold is shown (determined as 100X SD of the baseline), with each data point representing a single well run in quadruplicate for 5 biological replicates of TBI hippocampus, TBI cerebral cortex, sham-injury hippocampus, and sham-injury cerebral cortex. Tissue dilutions are indicated, with quadruplicate wells of 5 biological replicates evaluated at 10<sup>-3</sup>, 10<sup>-4</sup>, and 2 biological replicates at 10<sup>-5</sup>. Mouse tau KO brain homogenate was evaluated as a negative control, and synthetic fibrils generated from recombinant tau served as a positive control.

(F), (G) western blot and its quantification show that total KIBRA expression remained constant across all time points after TBI (Each group n = 3).

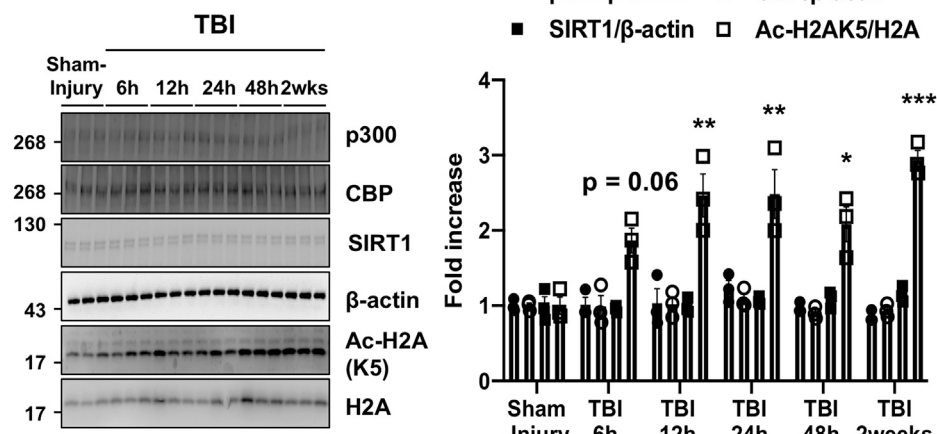
(H), (I) western blot and its quantification show that postsynaptic KIBRA expression, defined as post-synaptic density 95 protein fraction (PSD95), is not altered 24 hours or 2 weeks after TBI (Two pooled samples in each lane).

(J) Representative images show lack of axonal degeneration in cerebral cortex, hippocampus and hypothalamus of transgenic mice overexpressing wild-type human tau (scale bar = 5 μm), as expected.

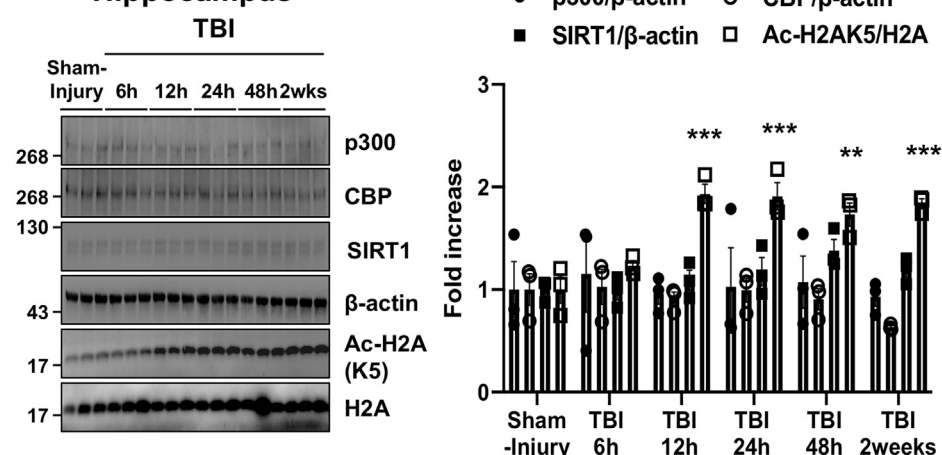
(K) Representative images show prominent axonal degeneration in cerebral cortex, hippocampus and hypothalamus of transgenic mice with human tau mutated to mimic acetylation of K274 and K281 (KQ) (TauKQ<sup>high</sup>), relative to nontransgenic littermates (scale bar = 5 μm).

(L) TauKQ<sup>high</sup> animals have reduced synaptic vesicle protein 2 (SV2) levels in stratum radiatum of hippocampus relative to nontransgenic littermates. (\*p < 0.05, Student's t test, scale bar = 30 μm).

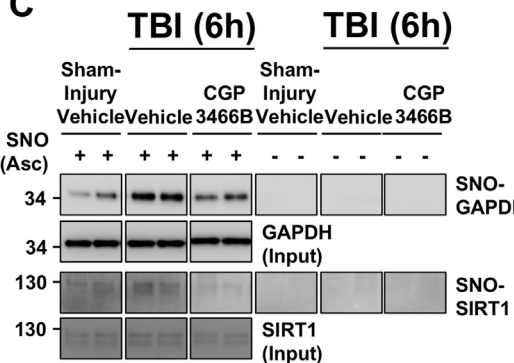
**A Cerebral cortex**



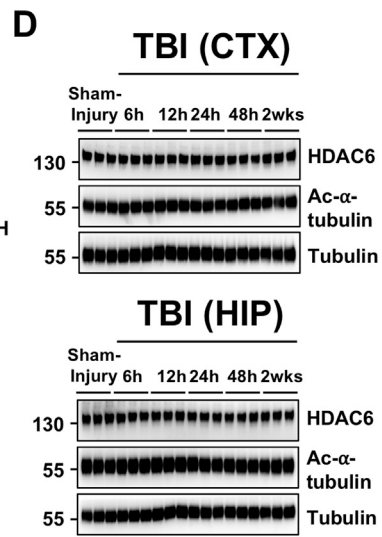
**B Hippocampus**



**C**



**D**



(legend on next page)

**Figure S3. TBI regulates p300/CBP and Sirt1 activity, but not HDAC6, related to Figure 2**

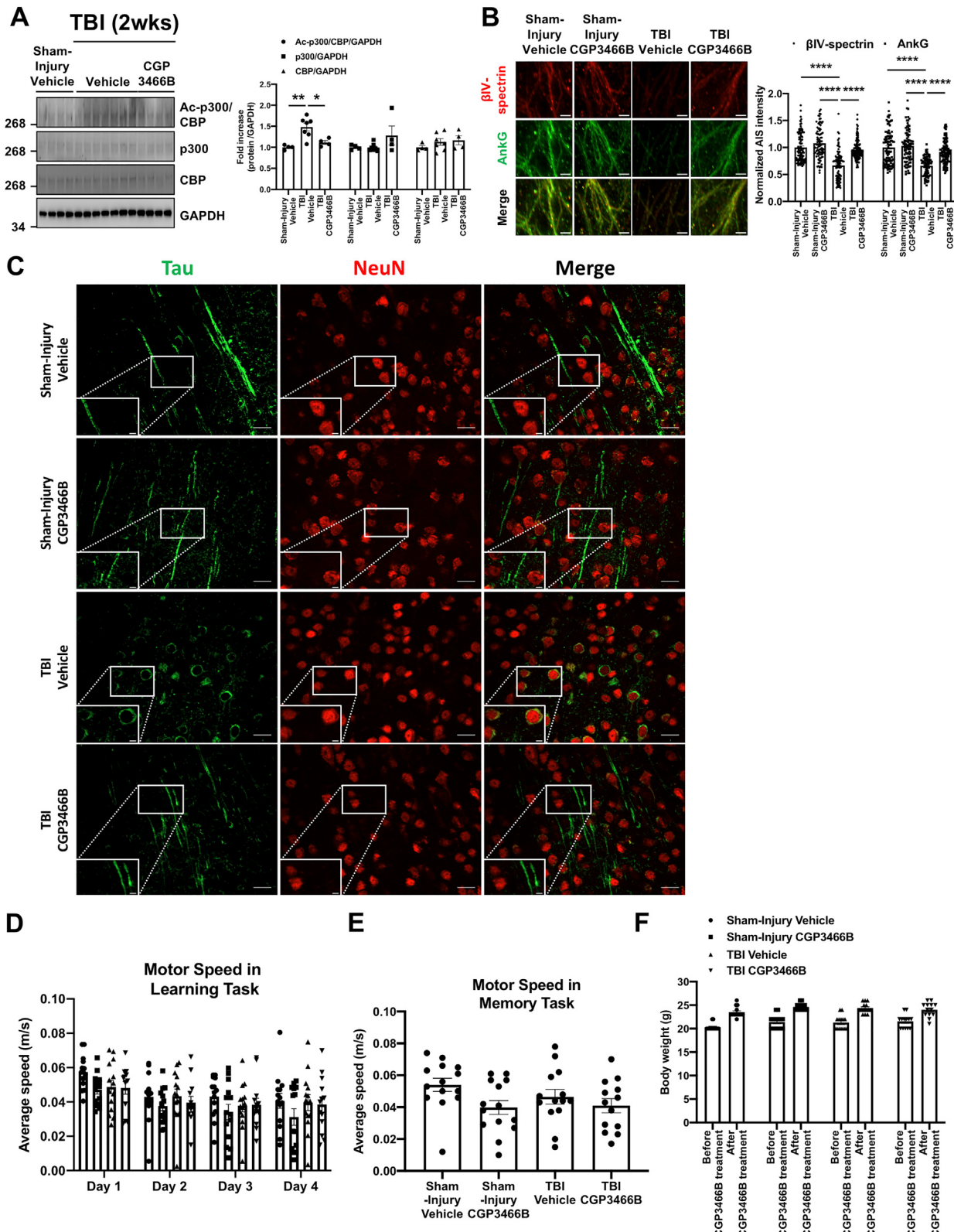
(A) western blot and its quantification show that TBI significantly increased acetylation of histone 2A lysine 5, a well-established substrate of p300/CBP and Sirt1, in the cerebral cortex in a time-dependent manner, without affecting expression levels of p300, CBP, or Sirt1.

(B) western blot and its quantification show that TBI significantly increased acetylation of histone 2A lysine 5, a well-established substrate of p300/CBP and Sirt1, in the hippocampus in a time-dependent manner, without affecting expression levels of p300, CBP, or Sirt1.

For (A) and (B), each group n = 3, \*p < 0.05, \*\*p < 0.01, \*\*\*p < 0.001 versus Sham-Injury group, one-way ANOVA with Dunnett multiple comparisons test.

(C) Treatment of CGP3466B inhibits S-nitrosylation of GAPDH and Sirt1 at 0.014 mg/kg (Each group n = 2, separation between squares represents cut in gel). Asc + represents SNO, and Asc - represents control.

(D) western blot and its quantification show that TBI does not affect expression of HDAC6, or its activity as measured by acetylated  $\alpha$ -tubulin in the cerebral cortex and hippocampus.



(legend on next page)

**Figure S4. CGP3466B treatment initiated 24 h after TBI blocks tau mislocalization and does not affect speed during behavioral testing or body weight, related to Figure 2**

(A) western blot and its quantification show that 0.014 mg/kg CGP3466B reduces ac-p300/CBP in cerebral cortex after TBI (Each group n = 4-7, \*p < 0.05, \*\*p < 0.01 versus TBI+Vehicle group, one-way ANOVA and Tukey's post hoc analysis).

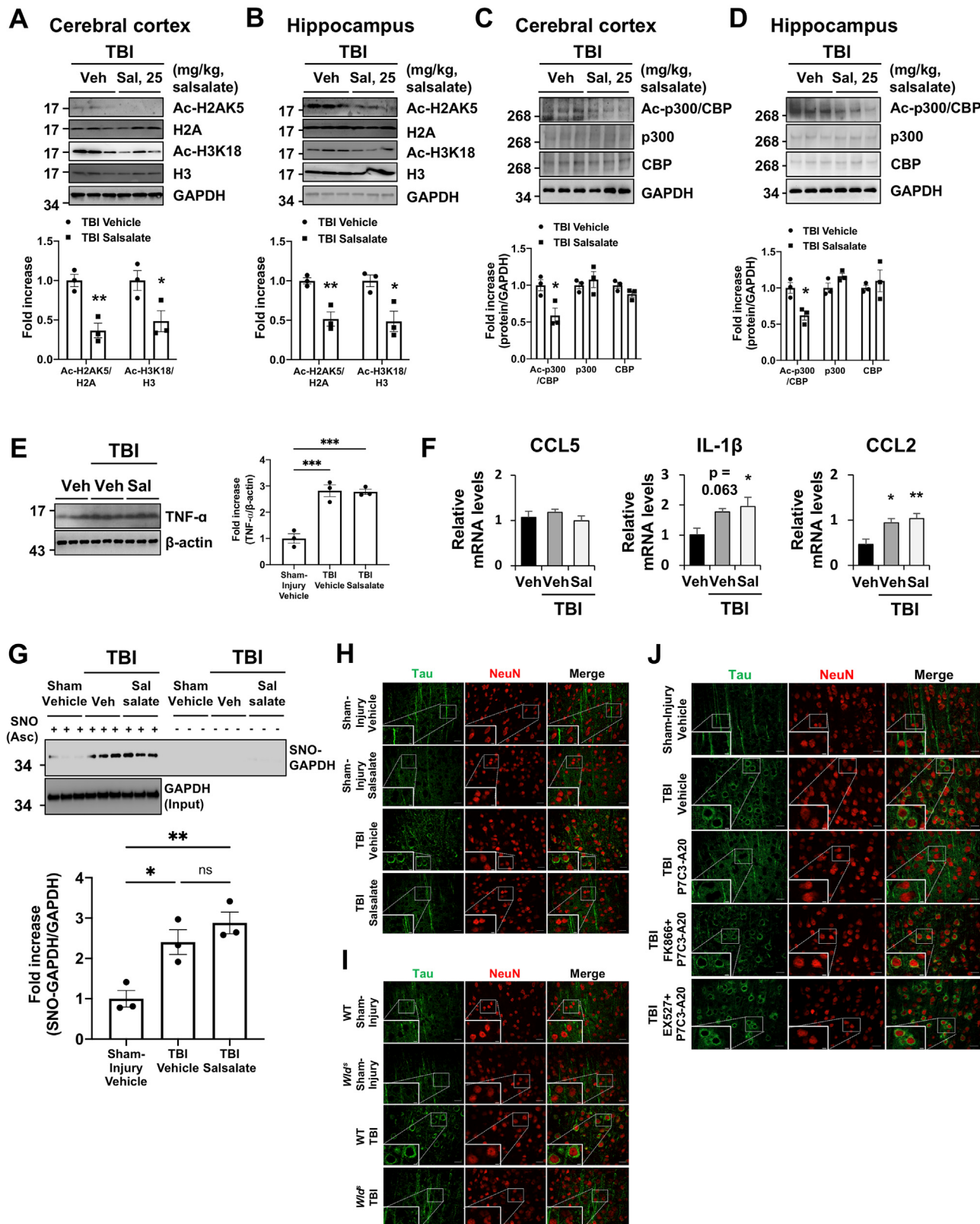
(B) CGP3466B protects mice from post-TBI AIS degradation in the hippocampus (Each group n = 3, \*\*\*p < TBI+Vehicle group, one-way ANOVA and Tukey's post hoc analysis, scale bar = 5 $\mu$ m).

(C) Images shown are lower power fields of tau localization in neurons from which higher power figures shown in Figure 2E were derived, with the higher power field shown in white box. (scale bar = 20  $\mu$ m for original image, 5  $\mu$ m for inset).

(D) CGP3466B treatment did not affect average speed during the learning phase of the Barnes maze task.

(E) CGP3466B treatment did not affect average speed during the memory phase of the Barnes maze task.

(F) CGP3466B treatment did not affect body weight.



(legend on next page)

**Figure S5. Low-dose salsalate inhibits p300/CBP activity, is devoid of any anti-neuroinflammatory effect after TBI, and does not affect S-nitrosylation of GAPDH after TBI; representative images of tau and NeuN, corresponding to main figures, related to Figures 3, 4, and 5**

(A), (B) Inhibition of p300/CBP by salsalate was assessed by measurement of acetylation of well-known substrates, H2AK5 and H3K18. Salsalate treatment significantly reduced levels of ac-H2AK5 and ac-H3K18 in cerebral cortex and hippocampus (Each group n = 3, \*p < 0.05, \*\*p < 0.01 versus TBI+Vehicle group, Student's t test).

(C), (D) western blot and its quantification show that acetylation of p300/CBP was also significantly reduced by treatment with salsalate (Each group n = 3, \*p < 0.05 versus TBI+Vehicle group, Student's t test).

(E) western blot analysis and its quantification show that the proinflammatory cytokine TNF-alpha is upregulated in the cerebral cortex in response to TBI injury, and that this increase is not affected by treatment with 25 mg/kg of salsalate. (Each group n = 3, \*\*\*p < 0.001 versus Sham-Injury+Vehicle group, one-way ANOVA and Tukey's post hoc analysis).

(F) qPCR analysis shows that IL-1 $\beta$  and CCL2 are upregulated in TBI-injured cerebral cortex, and that this increase is not attenuated by treatment with 25 mg/kg of salsalate. Levels of CCL5 were not affected by either TBI or salsalate. (Each group n = 3, \*p < 0.05, \*\*p < 0.01 versus Sham-Injury+Vehicle group, one-way ANOVA and Tukey's post hoc analysis).

(G) western blot and its quantification show that S-nitrosylation of GAPDH is not affected by treatment with 25 mg/kg salsalate. (Each group n = 3, \*p < 0.05, \*\*p < 0.01 versus Sham-Injury+Vehicle group, one-way ANOVA and Tukey's post hoc analysis). "Ascorbate (Asc) – negative control" shows specificity of signal in the SNO-resin-assisted capture technique.

(H), (I), (J) Images shown are lower power fields from which higher power figures shown in the corresponding main figures were derived, with the higher power field shown in white box. (scale bar = 20  $\mu$ m for original image, 5  $\mu$ m for inset). (H) Images for salsalate experiment in Figure 3C. (I) Images for *Wld<sup>S</sup>* experiments in Figure 4C. (J) Images for P7C3-A20 experiments in Figure 5D.

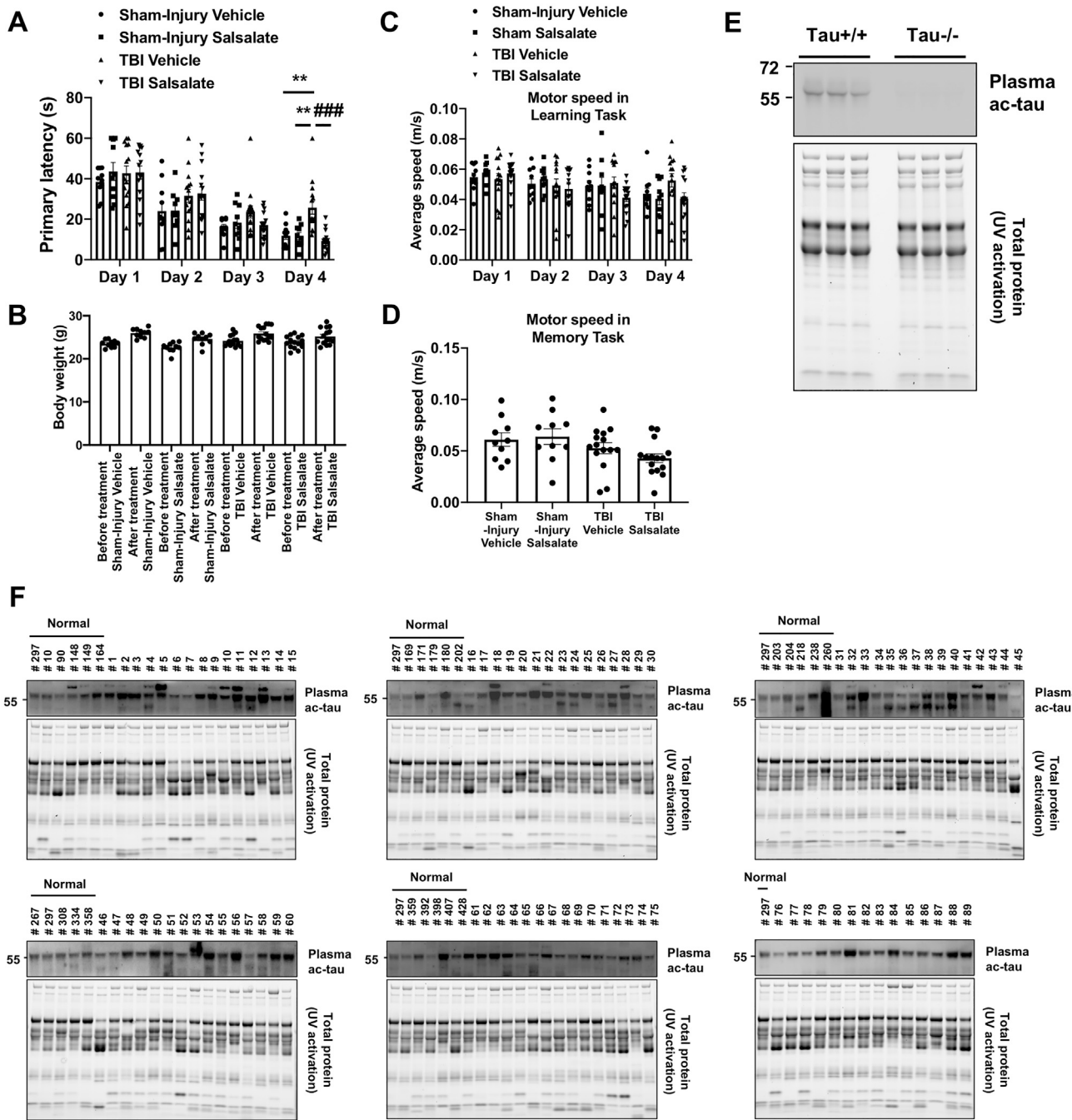


**Figure S6.** Low-dose salsalate treatment did not affect average speed in behavioral testing or body weight, and ac-tau antibody specifically recognizes ac-tau in both mouse and human plasma, related to Figures 3 and 6

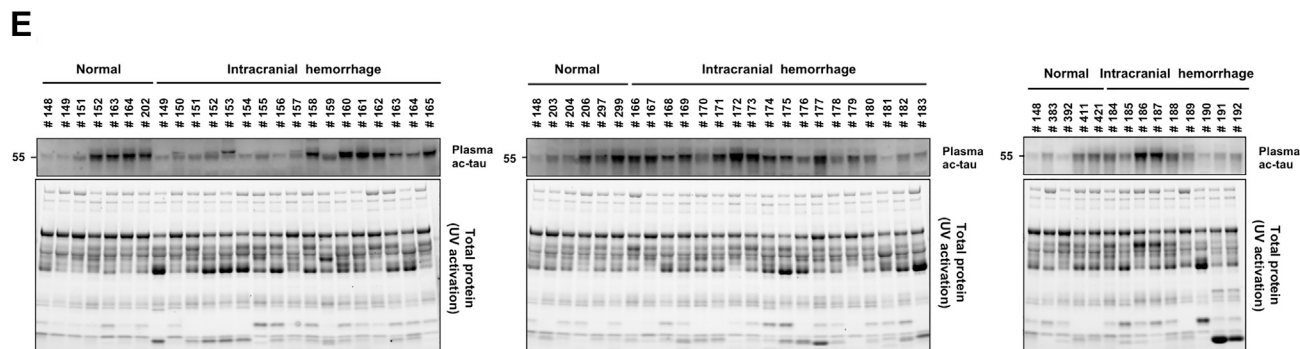
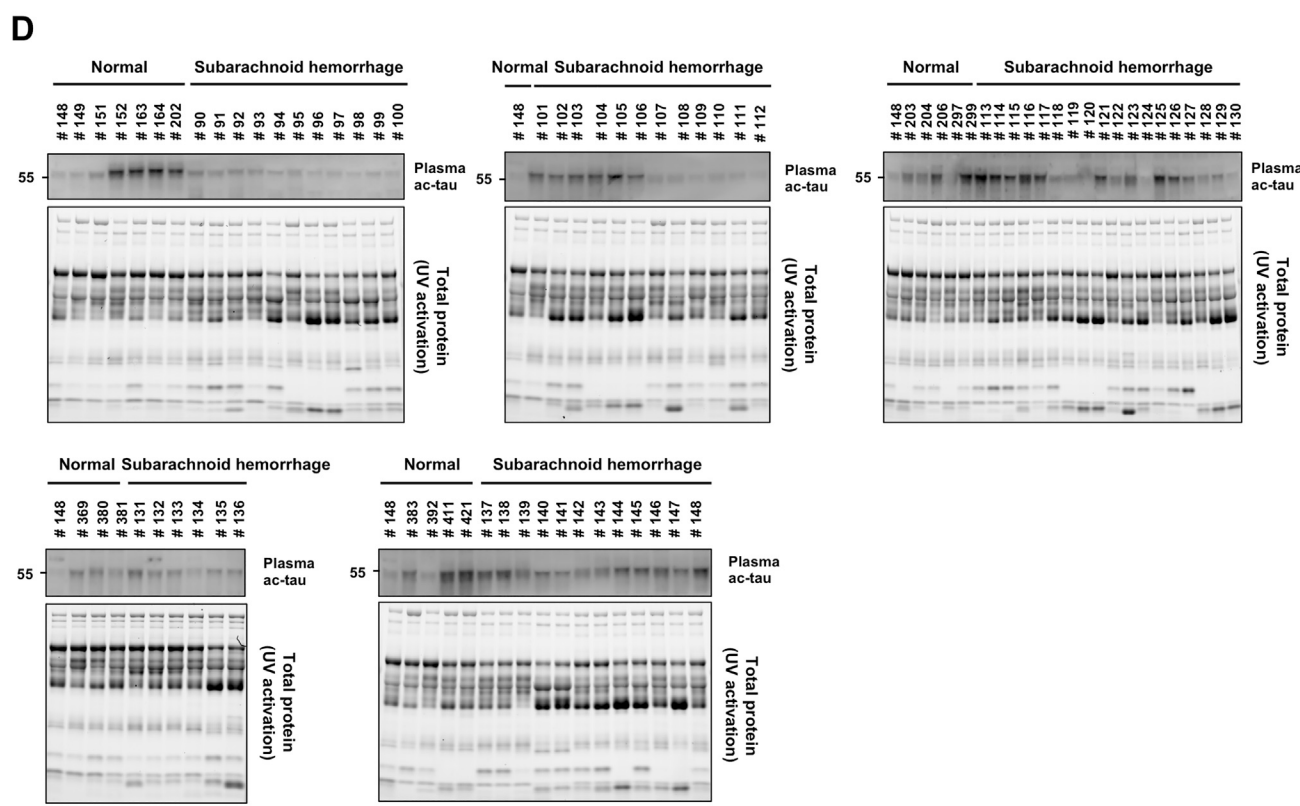
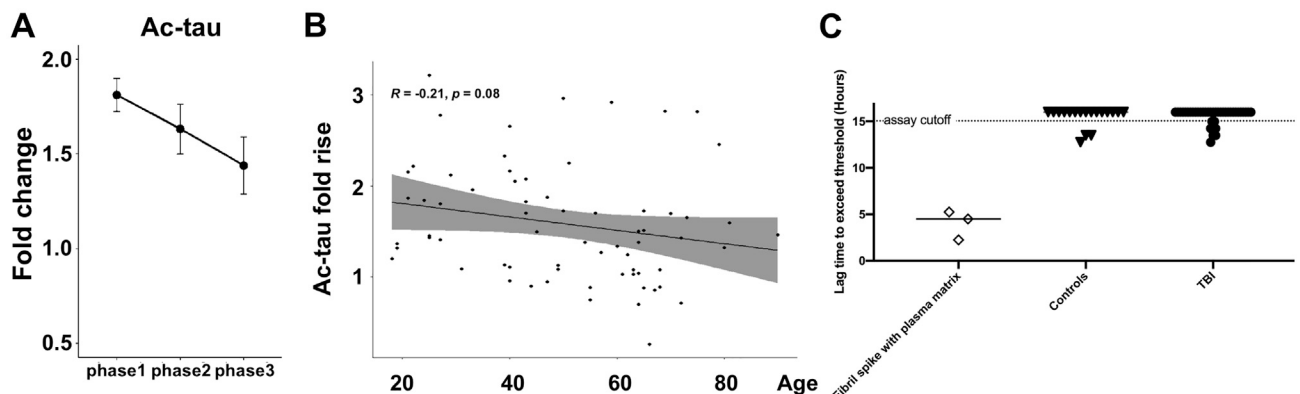
(A) Treatment of salsalate improved learning as measured by primary latency during the training period of the Barnes maze. (\*\*p < 0.01 versus Sham-Injury+Vehicle group, or Sham-Injury+Salsalate group, ### p < 0.001 versus TBI+Vehicle group, Repeated-measures two-way ANOVA for learning test).

(B) Body weight was not altered by treatment with salsalate.

(C), (D) Average speed was not affected by treatment with salsalate.

(E) Validation of plasma ac-tau using wild-type and tau knockout blood samples.

(F) Western blot for ac-tau in control (Normal) and TBI samples (all others). Subject # 260 was removed from the analysis due to the comorbid factor of acute myositis.



(legend on next page)

---

**Figure S7. Ac-tau in the populations studied was not associated with age or tau seeding, and showed no increase in subarachnoid or intracranial hemorrhage, related to Figure 6**

(A) TBI samples were obtained from 5 time points: T<sub>1</sub>, T<sub>3</sub>, T<sub>4</sub>, T<sub>5</sub> and T<sub>6</sub>. Since the availability of samples after T<sub>1</sub> was sparse, samples collected at T<sub>1</sub>, samples collected at T<sub>3</sub> and T<sub>4</sub>, and samples collected at T<sub>5</sub> and T<sub>6</sub> were grouped together as < 24 hours phase, 24–120 hour phase, and > 120 hours phase, respectively. Samples included mild (Glasgow Coma Score of 13 to 15), moderate ((Glasgow Coma Score of 9 to 12) and severe head injury (Glasgow Coma Score less than 8). After grouping, there were 44 (15 mild, 15 moderate, 14 severe), 28 (10 mild, 12 moderate, 6 severe) and 17 (5 mild, 2 moderate and 10 severe) samples at < 24 hours, 24–120 hours and at > 120 hours respectively. One sample at T<sub>3</sub> was discarded as the subject had a sample at T<sub>4</sub> as well. The mean values were fit by splines for better visualization. There was a decreasing trend in fold-rise of ac-tau values from the acute onset of injury (< 24 hour phase) to progression into the sub-acute stages of injury (24–120 hour phase and > 120 hour phase).

(B) There were no significant associations between age and the fold-rise in ac-tau ( $R = -0.21$ ,  $p = 0.08$ ).

(C) No significant tau seeding activity was detected in acute TBI plasma samples compared to controls. Plasma samples from acute TBI ( $n = 13$ ) and control cases ( $n = 7$ ) were analyzed by AD RT-QuIC. As a positive control, ~18 ng of synthetic fibrils (sFibril) was spiked into one of the control plasma samples, which was then used to seed the assay. Each data point indicates an individual well, analyzed in triplicate for each biological replicate. Lag time is the time required for the ThT fluorescence to exceed a threshold of 100X SD above the assay baseline before the assay cutoff, set at 15 h based on lag times to spontaneous amyloid formation in the negative controls.

(D) Western blot for ac-tau in control (Normal) and subarachnoid hemorrhage samples (all others).

(E) Western blot for ac-tau in control (Normal) and intracranial hemorrhage samples (all others).